International Journal of Pharmaceutics 651 (2024) 123790

Contents lists available at ScienceDirect

International Journal of Pharmaceutics

journal homepage: www.elsevier.com/locate/ijpharm

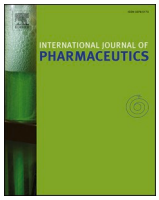

Printing a cure: A tailored solution for localized drug delivery in liver cancer treatment

Souha H. Youssef [a], Raja Ganesan [b], Marzieh Amirmostofian [c], Sangseo Kim [a], Ruhi Polara [b], Franklin Afinjuomo [a], Yunmei Song [a], Bradley Chereda [b], Nimit Singhal [e,f], Nirmal Robinson [b,d,1], Sanjay Garg [a,*,1]

[a] Centre for Pharmaceutical Innovation (CPI), University of South Australia, Adelaide, SA, Australia
[b] Centre for Cancer Biology, University of South Australia and SA Pathology, Adelaide, SA, Australia
[c] Clinical & Health Sciences, University of South Australia, Adelaide, SA, Australia
[d] Discipline of Medicine and the Faculty of Health Science, University of Adelaide, Adelaide, SA, Australia
[e] Royal Adelaide Hospital, Central Adelaide Local Health Network, Adelaide, SA, Australia
[f] Dept of Medicine, University of Adelaide, Adelaide, SA, Australia

ARTICLE INFO

Keywords:
3D printing
Liver cancer
5 Fluorouracil
Cisplatin
Personalized medicine

ABSTRACT

Adjuvant chemotherapy is highly recommended for liver cancer to enhance survival rates due to its tendency to recur frequently. Localized drug-eluting implants have gained traction as an alternative to overcome the limitations of systemic chemotherapy. This work describes the development of biodegradable 3D printed (3DP) bilayer films loaded with 5-fluorouracil (5FU) and cisplatin (Cis) with different infill percentages where the 5FU layers were 40%, 30%, and 30% and Cis layers were 10%, 15%, and 10% for films A, B, and C, respectively. The relevant characterization tests were performed, and the drug content of films was 0.68, 0.50, and 0.50 mg of 5FU and 0.39, 0.80, and 0.34 mg of Cis for films A, B, and C, respectively. Cis release was affected by the alterations to the film design, where films A, B, and C showed complete release at 12, 14, and 23 days, respectively. However, 5FU was released over 24 h for all films. The films were stable for up to two weeks after storage at 25 °C/65% relative humidity and four weeks at 4 °C where drug content, tensile strength, FTIR, and thermal analysis results demonstrated negligible alterations. The cytotoxicity of the films was assessed by MTS assays using HepG2 cell lines demonstrating up to 81% reduction in cell viability compared to blank films. Moreover, apoptosis was confirmed by Western Blots and the determination of mitochondrial cell potential, highlighting the potential of these films as a promising approach in adjuvant chemotherapy.

1. Introduction

Liver cancer continues to have a challenging prognosis with a very low survival rate representing the second lowest rate among various cancer types (Siegel et al., 2019). Surgical resection for liver cancer patients who have not reached advanced stages is recommended (Sherman et al., 2011, Marrero et al., 2018, Lubel et al., 2021). However, residual microscopic tumor cells risk relapse of the disease, studies showed residual cells were detected at resection margins of up to 46 % of patients (Nordlinger et al., 2013, Zhang et al., 2014, Inchingolo et al., 2019, Heimbach et al., 2018, Pan et al., 2023). As a result, adjuvant chemotherapy is administered showing improved clinical outcomes compared to surgery alone (Pinna et al., 2018, Kawai et al., 2018, Nishioka et al., 2018, Tsilimigras et al., 2021, Wang et al., 2017). The development of targeted drug delivery strategies has been driven by the undesirable side effects, limited bioavailability, and multi-drug resistance associated with systemic chemotherapy (Chidambaram et al., 2011). Localized drug delivery systems (DDS) have emerged as a promising approach to addressing these issues. Drug-eluting films are excellent candidates due to their flexibility and ease of handling.

The co-administration of 5-fluorouracil (5FU) and cisplatin (Cis) was found to exert a superior response rate in the treatment of liver cancer (Okamura et al., 2004, Kobayashi et al., 2006, Ueshima et al., 2010). 5FU and Cis are delivered clinically via hepatic arterial infusion

* Corresponding author.
E-mail address: Sanjay.garg@unisa.edu.au (S. Garg).
[1] These authors contributed equally to this work.

https://doi.org/10.1016/j.ijpharm.2024.123790
Received 17 October 2023; Received in revised form 20 December 2023; Accepted 4 January 2024
Available online 6 January 2024

chemotherapy in Japan, South Korea, and Taiwan (Kudo et al., 2018) and in other settings (Lazaros et al., 2012). The combination was also co-formulated in the form of a hydrogel for intraoperative chemotherapy for gastric cancer (Chen et al., 2023). Although the improved outcomes associated with the use of 5FU and Cis in several cancer types, no consistent protocol has been established regarding doses and administration methods which vary among institutes(Kengo et al., 2012). Some protocols administer 5FU and Cis sequentially(Ando et al., 2002), simultaneously(Ueshima et al., 2010), intermittent administration of 5FU with a daily low dose Cis drip(Kanetaka et al., 2012, Terashima et al., 2003), and a single day Cis dose administration with a continuous 5-day 5FU infusion (Andreadis et al., 2003). Considering, 5FU has a short half-life and is cleared rapidly from the body reducing its bioavailability, and Cis suffers from serious dose-limiting toxicity, the incorporation of this combination in localized DDS could potentially overcome these limitations and improve therapeutic outcomes.

There are several methods of fabricating films including solvent casting (Karki et al., 2016), electrospinning (Zhang et al., 2014), and hot melt extrusion (Repka et al., 2005). Nonetheless, a novel approach different from the "one size fits all" is necessary due to the heterogeneous nature of cancer. Consequently, the adoption of the 3D printing technique has acquired substantial prominence in recent years as it offers the flexibility of producing customized films tailored to meet individual patients' needs. Customization parameters include flexibility in designs allowing for implantation in irregular cavities (Lim et al., 2018), modulating drug release profiles, and creating products with multi-layers, multi-compartments, and multi-components through digital control (Preis et al., 2015). A semi-solid extrusion (SSE) printer was adopted in this work due to its simplicity, and the application of mild printing conditions. The literature revealed some 3D printed (3DP) implants for delivering 5FU individually targeting pancreatic (Yi et al., 2016), cartilage (Salmoria et al., 2017), and oesophageal (Fouladian et al., 2020) cancers and in combination with NVP-BEZ235(reversible PI3K/mTOR inhibitor) (Yang et al., 2020) and gold nanoparticles (Di Luca et al., 2022). Cis-loaded implants were also formulated using 3D printers individually(Jing et al., 2021) and in combination with doxorubicin (Qiao et al., 2019), and ifosfamide, methotrexate, and doxorubicin (Wang et al., 2020) for the treatment of breast and bone cancers, respectively. To the best of our knowledge, films with the proposed drug combination have not been reported to date.

Despite the constant advancements in the pharmaceutical field contributing to improvements in treatment outcomes and patients quality of life, the pharmaceutical industry has emerged as one of the primary contributors to the generation of chemical waste and pollutants, along with substantial emissions of greenhouse gases (Belkhir and Elmeligi, 2019, Elbadawi et al., 2023). Considering the development process of a pharmaceutical product, synthesis, formulation, and analysis are involved. The formulation optimization requires many trials and analytical experiments, generating considerable quantities of solvent waste and energy consumption. Therefore, a focus on the environmental impact of the procedures performed during the development process is desirable.

In this work, biodegradable 3DP bilayer films, loaded with 5FU and Cis were developed for the first time. The relevant characterization and stability testing was performed to ensure the formulation's integrity. The influence of different infill percentages on the drug release trends was also evaluated to assess the possibility of modulating drug release. Moreover, MTS assays on HepG2 cells were carried out to support the feasibility of using these films to treat liver cancer, and the results were supported by Western Blotting and other imaging techniques. This research was performed with environmental awareness focusing on minimizing the environmental implications where possible. The analysis methods used throughout this research were assessed using the Analytical GREEnness Metric Approach and Software (AGREE) (Pena-Pereira et al., 2020) and analytical ecoscale (Gałuszka et al., 2012). Secondly, the 3D printing process was optimized for greenness through evaluation and modification based on scores obtained by the index of Greenness Assessment of Printed Pharmaceuticals (iGAPP), a tool developed and validated in our previous study (Youssef et al., 2022).

2. Materials and methods

2.1. Materials used in the development of 3DP films

Polycaprolactone (PCL), molecular weight 80 kDa, and sodium dodecyl sulfate (SDS) were purchased from Sigma-Aldrich (a subsidiary of Merck, NSW, Australia). Poly (lactic-co-glycolic acid) (PLGA), ratio 1:1, acid end cap, and a molecular weight of 15 kDa was procured from Nomisma Healthcare (Gujarat, India). Tetrahydrofuran (THF) was obtained from RCI labscan (SA, Australia). Methanol, dichloromethane (DCM), acetonitrile, N, N-dimethylformamide (DMF), acetone, sodium dihydrogen phosphate, and potassium chloride were purchased from Merck (Vic, Australia). Triethyl citrate (TEC) was bought from Alfa Aesar (Lancashire, United Kingdom). 5FU and Cis were purchased from Shandong Bouyan Pharmaceutical Co. Ltd. (Shandong, China). Sodium chloride was acquired from Medisca (NY, USA) and disodium hydrogen phosphate from Honeywell (Germany). Water used in the experiments was Milli-Q water (Sartorius – Göttingen, Germany). The human hepatoma cell line HepG2 was purchased from ATCC (USA).

2.2. Preparation of 3DP bilayer films

2.2.1. Bilayer film design

The outline of the bilayer film design was performed using Autodesk Inventor® Professional 2021 (Autodesk Inc., USA). Films were designed as squares (20 mm × 20 mm) for all the experiments except for determining tensile strength where films were rectangular (40 mm × 10 mm) with 0.5 mm thickness per layer. The files were created as stereolithography (.stl) files and converted into G-code files for processing by the 3D printer software. The infill patterns - grid (30% and 40% infill), and honeycomb (10 % and 15% infill) were designed using Bio X, Cellink software, BIO X Heart OS v1.8.2 + 193 (rev1). Table S1 shows the designs used in this study.

2.2.2. Preparation of printing ink

To dissolve PLGA and TEC (Table 1), they were mixed in THF at 50 °C while maintaining a constant stirring speed of 500 rpm (Heidolph-MR Hei, Germany). Subsequently, DMF was used to dissolve 5FU or Cis, added portion-wise to the previous solution, and stirred further for an hour. Finally, PCL was introduced to the mixture and subjected to continuous mixing at 350 rpm and 50 °C for 2 h. The mixing containers were covered to prevent solvent evaporation during the preparation process. Blank printing inks were prepared similarly without the addition of 5FU or Cis.

2.2.3. 3D printing of bilayer films

The printer used was based on a pressure-assisted microsyringe technique connected to dual printing heads (Bio X, Cellink, Gothenburg, Sweden). An aliquot of each of the prepared printing inks (2 ml) was transferred to a 3D printer cartridge with a 25 G nozzle (inner diameter: 250 μm). The first layer was printed under pressure of 50 kPa, printing

Table 1
Amounts of components used for the preparation of the printing ink.

The developed films		PCL (g)	PLGA (g)	TEC (μl)	Drug (mg)	DMF (ml)	THF (ml)
Blank	Layer 1	2	1	350	0	1	9
	Layer 2	2	0	0	0	1	9
Drug - loaded	Layer 1 (5FU)	2	1	350	40	1	9
	Layer 2 (Cis)	2	0	0	20	1	9

cartridge temperature of 40 °C, and a printing speed of 5 mm/s, the film was allowed to partially harden before printing the second layer. The printing head was manually calibrated to enable the second layer to be positioned correctly and printing was performed using a pressure of 55 kPa, a printing cartridge temperature of 40 °C, and a printing speed of 5 mm/s. Both layers were printed on a printing bed at room temperature (RT) and then left to dry at RT for 24 h. Fig. 1 shows a schematic diagram of the printing process. The different film designs are summarized in Table 2.

2.3. Differential Scanning calorimeter (DSC)

Accurately weighed samples (PCL, PLGA, 5FU, Cis, blank, and drug-loaded 3DP bilayer films) (~5 mg) were placed in aluminum pans and sealed hermetically. Samples were heated to 350 °C at a rate of 10 °C/min starting from 25 °C under nitrogen (50 ml/min), and DSC charts were generated using Discovery DSC 2920 (TA Instruments, New Castle, DE, USA).

2.4. Fourier transform infrared (FTIR)

The printed films (blank and drug-loaded) and their components (PCL, PLGA, 5FU, and Cis) were scanned with an FTIR spectrometer coupled with a UATR accessory (Spectrum Two, Perkin Elmer Inc, USA). The obtained spectra were within the range of 330 to 4000 cm^{-1} by applying 16 scans. F. Menges "Spectragryph - optical spectroscopy software", Version 1.2.16.1, 2022, http://www.effemm2.de/spectragryph/ was used for illustration purposes.

2.5. Scanning electron microscopy (SEM)

The SEM apparatus used was a Zeiss Merlin Field Emission Gun Scanning Electron Microscope (Jena-Germany) model. Sample preparation involved placing 3DP blank and drug-loaded films on double-sided tape, then sputter coating was performed with platinum (approximately 5 nm), accelerating voltage of 2–5 kV was applied. Samples of pure 5FU and Cis were also examined using the same procedure.

Table 2
3DP bilayer film designs.

Films	Layer 1		Layer 2	
	Infill pattern	Infill density	Infill pattern	Infill density
Film A	Grid	40%	Honeycomb	10%
Film B	Grid	30%	Honeycomb	15%
Film C	Grid	30%	Honeycomb	10%

2.6. Quantification of 5FU and Cis by HPLC

A previous study was conducted to develop an analysis method for the simultaneous determination of 5FU and Cis by HPLC(Youssef et al., 2021). Separation was performed with C18 column, Phenomenex® (250 mm × 4.6 mm, Luna® 5 µm). A mixture of 98% 0.5 mM sodium dodecyl sulfate solution (pH 2.5) and 2% methanol was used as a mobile phase and pumped through the HPLC system at a rate of 0.5 ml/min, the injection volume was 10 µl, and the use of photodiode detector identified the peak of 5FU and Cis at 265 and 210 nm, respectively.

2.7. Determination of drug content in printed films

Films (20 mm × 20 mm) were dissolved in 1 ml DCM, 5 ml of 0.9% saline solution, and 5 ml of mobile phase were then added, and the mixture was vortexed for 15 min. The mixture was left to stand for 2 h, then an aliquot of 200 µl was withdrawn from the aqueous layer and analyzed by the HPLC method. The accuracy of the extraction method was determined by carrying out the extraction steps using a known amount of 5FU and Cis. The uniformity of drug contents in the printed films was determined by quantifying the drug contents of 3 different freshly printed bilayer films (20 mm × 20 mm) and the results were presented as the amount of drug (mg) / film ± SD.

2.8. Determination of residual solvents in films

THF and DMF were used in preparing the printing inks. Films (Layer 1: 40% infill; Layer 2: 15% infill) representing maximum pattern density with dimensions 20 mm × 20 mm were used.

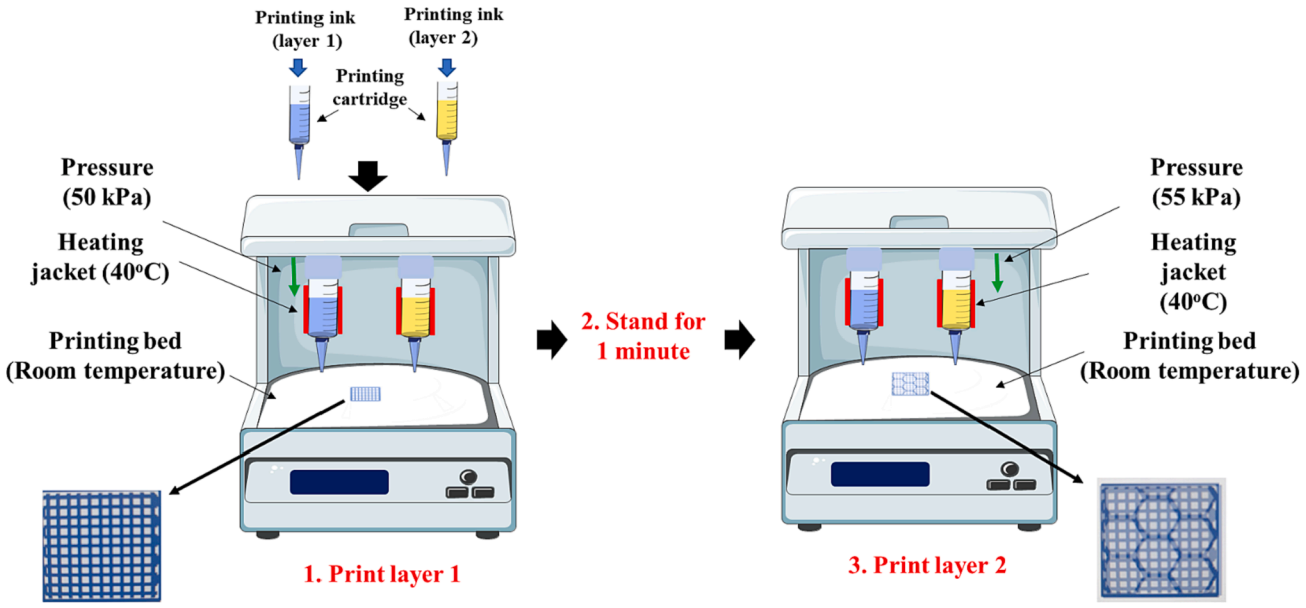

Fig. 1. A schematic diagram representing the printing process of the bilayer films (Parts of the figure were drawn using pictures from Servier Medical Art. Servier Medical Art by Servier is licensed under a Creative Commons Attribution 3.0 Unported License (https://creativecommons.org/licenses/by/3.0/ accessed on 3 July 2023).

2.8.1. Quantification of THF in 3DP films

Gas chromatography-tandem mass spectrometry (GC-MS/MS) was used for the quantification of the residual THF in the prepared films (Isaacson et al., 2006). The printed films were dissolved in 0.5 ml acetone and then filtered using a PTFE membrane (0.45 μm), THF residues were then quantified using GC–MS/MS. The chromatographic conditions are summarized in Table S2.

2.8.2. Quantification of DMF in 3DP films

Residual amounts of DMF were determined by a previously reported HPLC method (Arafat et al., 2020). Briefly, 3DP films were dissolved in 0.5 ml THF then an equal volume of water was added. The solution was centrifuged for 5 min at a speed of 10,000 rpm (Eppendorf Centrifuge 5415R - Germany). The supernatant was taken and filtered using a 0.45 μm PTFE membrane. An aliquot of 200 μl was injected into the HPLC system. The chromatographic conditions are summarized in Table S3.

2.9. Determination of in vitro drug release profiles

5FU and Cis release behaviors from the printed films were studied by simulating physiological and cancerous tissue conditions regarding pH variation at pH 7.4 and 6.9.

2.9.1. Determination of the stability of 5FU and Cis in PBS

The stability of 5FU and Cis in combination for the duration of the *in vitro* release study was examined by placing a mixture of 5FU and Cis of known concentration diluted with PBS (pH 7.4 and 6.9) in a horizontal shaker (37 °C, 175 rpm). Aliquots were taken on the 7th, 14th, and 25th days and analyzed by HPLC to quantify 5FU and Cis contents. Calculations were performed to obtain recovery percentage (R%) ± SD.

2.9.2. In vitro release study

Freshly printed bilayer films A, B, and C (20 mm × 20 mm) were submerged in 50 ml falcon tubes with 10 ml PBS (pH 7.4 and 6.9). The tubes were wrapped in aluminum foil for protection from light and then placed in a horizontal shaker (37 °C, 175 rpm). At pre-determined time points, 1 ml of release medium was collected and replaced with fresh PBS. The content of 5FU and Cis in the withdrawn samples was quantified by the aforementioned HPLC method.

2.9.3. Mathematical modelling

The mechanism of the release of the drugs was assessed by fitting the *in vitro* release data against mathematical models using DDSolver (Microsoft Excel add-in software). The adjusted coefficient of determination (R^2), the root mean squared error (RMSE), and the Akaike Information Criterion (AIC) were obtained to define the best-fitting model.

2.10. Stability studies

Stability studies for the printed films were performed under two storage conditions with different temperatures and humidity levels. Drug-loaded printed films were individually wrapped with a plastic layer and then sealed in aluminum bags. They were then stored under the following conditions:

A. Controlled stability chamber at 25 °C/relative humidity of 65%
B. Refrigerated at 4 °C

Samples were retrieved at predetermined time points and the drug content, FTIR, DSC, thermogravimetric analysis (TGA), and tensile strength examination were performed on the films. The tensile strength of the films was defined using a texture analyzer (TA. XTplus Texture analyzer, Stable Micro Systems, Surrey, UK), with load cell weight of 10 kg following ASTM D882 standard (Film dimensions: 40 × 10 mm, n = 3). Films were stretched at a strain rate of 5 mm/s until rupture. Results were analyzed statistically to compare changes in the tensile strength of stored films to freshly printed ones. For TGA (Discovery TGA 550, TA Instruments, New Castle, DE, USA), samples weighing ~ 6 mg were deposited in platinum pans and exposed to heat under nitrogen gas flow at a rate of 10 °C/min up to 600 °C.

The DSC, FTIR, and drug content of the stored films at the selected time points were assessed as described under each test in sections 2.3, 2.4, and 2.7, respectively. The obtained results were compared to the results obtained from freshly printed films.

2.11. Statistical analysis

Statistical analysis was performed using GraphPad Prism Software (version 9.5.1, CA, USA). The results from the *in vitro* release studies and stability studies were analyzed using a one-way analysis of variance followed by Tukey's multiple comparison test. The results were obtained from three independent experiments, and the difference was considered statistically significant when the p-value was < 0.05.

2.12. In vitro cytotoxicity

2.12.1. MTS assay

2.12.1.1. Cell culture conditions. HepG2 cells were grown at 37 °C in a humidified 5% CO_2-containing atmosphere in D10 media [DMEM supplemented with 10% of heat-inactivated Fetal Bovine Serum (FBS) (Cytiva, Hyclone FBS, Australia) and 100 U/ml penicillin and streptomycin (GIBCO)]. All the cells were constantly checked for mycoplasma contamination using MycoAlert Mycoplasma Detection Kit (Lonza, LT07-318) and were negative for mycoplasma.

The effect of 5FU and Cis treatment on HepG2 cell viability was examined using 3-(4,5-dimethylthiazol-2-yl)-5-(3-carboxymethoxyphenol)-2-(4-sulfophenyl)–2H-tetrazolium (MTS) which forms a purple formazan in the presence of phenazine methosulfate (PMS). In brief, the HepG2 cells (1×10^4 cells per well in 100 μl of D10 medium) were seeded in flat bottom 96 wells plates (Corning, Falcon® 96-well Clear Flat Bottom TC-treated Culture Microplate) 16–20 h before the treatment. The cells were treated with 5FU and Cis at different concentrations for 24 h, and the cell viability was measured using MTS Cell Proliferation Assay (Promega CellTiter 96® AQueous One Solution Cell Proliferation Assay, G5421). The absorbance was measured using an EPOCH microplate spectrophotometer (BioTek, USA) using Gen5 software. For the extract dilution test (EDT), the extracted medium was diluted with D10 medium at a 1:1 ratio and added to the cells. For the direct contact test (DCT), the 3DP bilayer films were placed on top of the medium and incubated for 24 h. The films were removed at the desired time points, and the MTS assay was conducted as per protocol.

2.12.2. Cell imaging

The cell morphological cytotoxic effects of 5FU and Cis on HepG2 cells treated with EDT and DCT methods were imaged using EVOS FL Cell Imaging System with the bright filed microscope at 20x magnification at various time points and concentrations.

2.13. IncuCyte cytotox green assay

Cell proliferation and cell confluency were determined with live-cell imaging using the Sartorius IncuCyte Live Cell Imaging System (Essen Bioscience, Ann Arbor, MI, USA). In brief, HepG2 cells ($1\text{-}4x10^4$) were seeded per well in 100 μl D10 medium on a 96-well plate. The cells were incubated overnight at 37 °C in a 5% CO_2 humidified incubator before 5FU and Cis treatment. The treatment was performed by EDT and DCT in a D10 medium containing 250 nM of Cytotox Green. The cells were immediately transferred to Satorius IncuCyte Live Cell Imaging System. Each treatment condition included a triplicate of wells, where 4 fields of view per well were imaged at 3 h intervals for 48 h. The images and data

were analyzed using Incucyte software.

2.14. Western blot

The protein expression upon 5FU and Cis treatment was measured by standard immunoblotting. The HepG2 cells were cultured in a 6-well plate (Falcon® 6-well Clear Flat Bottom TC-treated, 353046) at a density of 1×10^6 cells and treated by EDT and DCT methods for 24 h. Following the treatment, the total protein was extracted from cells by Radioimmune precipitation assay lysis buffer (RIPA buffer, 50 mM Tris-HCl pH 8.0, 150 mM NaCl, 1% Triton X-100, 0.5% sodium deoxycholate, 0.1% SDS, 1 mM EDTA, containing Halt protease and phosphatase inhibitor mixture (Thermo Fisher Scientific. Australia, 78443). A total of 30 μg of lysate was separated in 4–20% Precast Mini-PROTEAN TGX stain-free protein Gel (BioRad, 4568094), and probed for cleaved PARP (9544), cleaved caspase-3 (9661) and GAPDH (2118) (Cell Signaling Technology). The blots were developed using Image Quant™ LAS 4000 (GE Healthcare).

2.15. Mitochondrial membrane potential

The cell-permeable dye, Tetramethylrhodamine, ethyl ester (TMRE) was used to evaluate the mitochondrial membrane potential of 5FU and Cis-treated HepG2 cells. Briefly, $0.25x10^6$ HepG2 cells were seeded on a 12-well plate (Falcon® 12-well Clear Flat Bottom TC-treated, 353043) and treated by EDT and DCT methods. The cells were stained with TMRE (50 nM) 24 h post-treatment and incubated for 20 min at 37 °C in the dark. The medium was removed, and the cells were gently washed twice with PBS. The cells were trypsinized and resuspended in PBS to get the cells in a single-cell suspension. Samples were run on the Cytoflex S (Beckman Coulter, Lane Cove, Australia), using the 561 nm laser-line (30mW) and 585/42 bandpass filter. Scatter was measured on the blue laser line (40mW). Flow cytometric data were analyzed using FCS Express 7 (De Novo Software, Pasadena, CA, USA).

2.16. Greenness assessment of the formulation development process

The analysis methods for the concurrent determination of 5FU and Cis, residual DMF, and residual THF were assessed using AGREE, and the results were complemented by calculating the analytical eco-scale score. The 3D printing process was scored by the iGAPP. The results were demonstrated as color-coded pictograms and corresponding scores.

3. Results and discussion

3.1. Preparation of 3DP bilayer films

3.1.1. Polymer selection for printing feed

The selection of PCL and PLGA was based on their printability and biodegradation (Abdella et al., 2021, Bassand et al., 2023). Our previous study showed that blending PCL and PLGA helped in overcoming their limitations when used individually, such as the low degradation rate of PCL and unsuitable mechanical properties of PLGA (Youssef et al., 2023). Although PCL has suitable mechanical properties, the addition of PLGA caused increased toughness of the films, consequently, triethyl citrate was added to restore the flexibility of the films. Moreover, the blending was found to reduce the burst release of 5FU (Youssef et al., 2023). A PCL: PLGA blend (2:1, w/w) was used in preparing the 5FU loaded printer feed (also referred to as printing ink) for layer 1. On the other hand, adding PLGA to the Cis-containing feed caused the degradation of Cis during the preliminary *in vitro* release studies, therefore, PLGA was eliminated from the Cis printer feed. These findings align with reported results which described that the degradation products of PLGA during incubation into its constituting monomers (lactic acid and glycolic acid), created an acidic microclimate as low as pH 2.8 causing instability of incorporated acid-labile drugs (Ding and Schwendeman, 2008, Schwendeman, 2002). The chemical stability of Cis is pH-dependent, where it has been proven to show stability at a pH range of 3.5–5.5 (Karbownik et al., 2012).

3.1.2. Printing parameters

Each layer of the developed films had a different infill pattern, grid and honeycomb for layers 1 and 2, respectively. The different infill patterns were found to provide the optimal design in terms of maintaining the film's structure when printed on top of each other. Different infill percentages were attempted aiming to modulate the drug release; thus, films A, B, and C were printed, as shown in Fig. 2.

The printing parameters were optimized where pressures ranging from 35 to 55 kPa for layer 1 and 40 to 60 kPa for layer 2 were tested. It was found that pressures below these ranges did not allow the flow of the ink through the printing nozzles. In contrast, greater pressures resulted in films of poor architecture with inconsistent pore sizes. Figure S1 shows the optimization of the applied printing pressure as it increased by 5 kPa increments. The viscosity of the printing ink for layer 2 was slightly higher than layer 1 due to the absence of triethyl citrate, therefore, a higher pressure was required. The best bilayer film (iv) was obtained upon applying 50 and 55 kPa for layers 1 and 2, respectively.

The printing speed also contributed to the resolution of the final product. Layer 1 was printed at printing speeds starting at 12 mm/s then the speed was reduced until an acceptable film was produced. Although faster printing is considered more efficient, it affected the integrity of the film, as demonstrated in Figure S2, a speed of 5 mm/s (film v) was found to be suitable. Lowering the speed beyond 5 mm/s was not attempted as it would prolong the printing process unnecessarily.

Furthermore, 25 G (internal diameter 250 μm) and 22 G (internal diameter 410 μm) were used to print the bilayer films, and 25 G nozzles were selected for the improved resolution of the bilayer design (Figure S3) over 22 G nozzles.

Finally, the temperature of the printing cartridges was set at 40 °C to avoid the solidification of the printing ink at the nozzle tip causing blockage.

The films were dried at RT as exposing films to higher temperatures risks softening the films and altering the geometry of the films' designs.

3.2. Characterization of 3DP bilayer films

3.2.1. FTIR

The FTIR spectra of the films and their components are demonstrated in Fig. 3.

The spectra for PCL, PLGA, and 5FU were extensively discussed in a previous study and the obtained results in this study were similar to the reported ones (Youssef et al., 2023), the results are summarized in Table S4. Cis showed peaks at 3281–3201 cm^{-1} and 1622–1541 cm^{-1} corresponding to asymmetric and symmetric stretching of amino groups and asymmetric and symmetric bending of HNH, respectively (Alkahtani et al., 2021). Peaks at 468 cm^{-1} and 340 cm^{-1} were observed representing bonds between platinum-ammonium, and platinum-chloride, respectively (Ebrahimi Shahmabadi et al., 2014). Upon investigating the 3DP films, characteristic peaks of PCL (2942, 2862, 1724, 1241, and 1176 cm^{-1}), and PLGA (2992, 1746, 1090–1173 cm^{-1}) were identified in 3DP blank bilayer films. Upon studying the spectra of the drug-loaded bilayer films, PCL and PLGA peaks were noted, however, several peaks related to 5FU exhibited similarities to the blank film owing to shared bands between the polymers and the drug. For instance, the presence of peaks at 2940 cm^{-1} and 1724 cm^{-1}, correspond to C–H and C = O, respectively (Arafat et al., 2021). Additionally, the 1241 cm^{-1} band associated with C-N in 5FU overlapped with PCL C-O-C groups and 1177 cm^{-1} for C-F with C-O-C groups from PLGA and PCL (Ashour et al., 2019). The low drug content in the films may have resulted in weak signals, which could have been overshadowed by signals from other elements in the sample (Chan and Kazarian, 2006). In contrast, characteristic peaks of Cis were observed in the drug-loaded

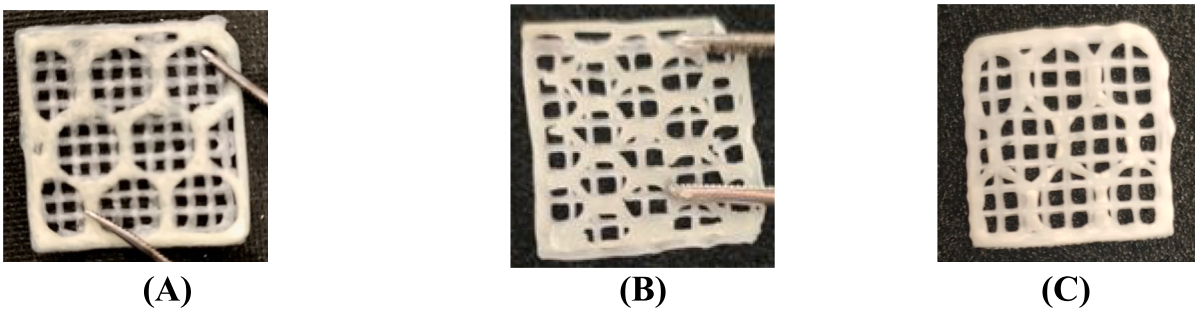

Fig. 2. 3DP bilayer films (A) Film A; layer 1: 40% infill grid pattern and layer 2: 10% infill honeycomb pattern (B) Film B; layer 1: 30% infill grid pattern and layer 2: 15% infill honeycomb pattern (C) Film C; layer 1: 30% infill grid pattern and layer 2: 10% infill honeycomb pattern.

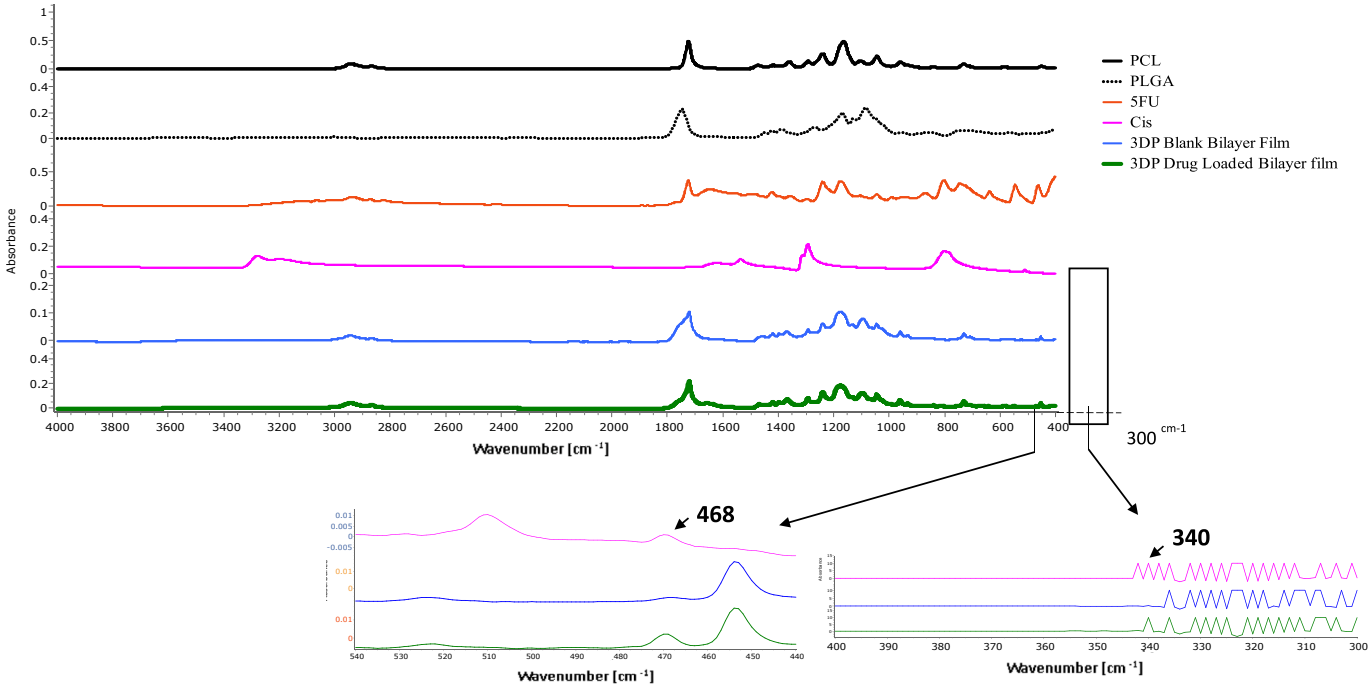

Fig. 3. FTIR spectra of PCL, PLGA, 5FU, Cis, blank 3DP bilayer film, and drug-loaded 3DP bilayer films.

films, such as the presence of peaks at 1643 cm^{-1}(asymmetric and symmetric bending of HNH) and 340 cm^{-1}(Pt-Cl) which were not prominently visible in the blank film. No new peaks were detected, suggesting the absence of chemical interactions between the film's components.

3.2.2. DSC

The DSC of the components of the drug-loaded film (PCL, PLGA, 5FU, and Cis) were studied (Fig. 4). PCL, 5FU, and Cis demonstrated sharp endothermic peaks at 57.2, 284, and 320 °C representing their melting points as previously reported in the literature (Alam et al., 2014, Youssef et al., 2023). Moreover, PLGA presented a degradation peak at 295 °C with no melting transition suggesting that the polymer exhibits an amorphous structure (Gentile et al., 2014). The absence of distinct peaks corresponding to 5FU and Cis in the drug-loaded bilayer films may indicate that the drugs were either molecularly dispersed within the polymer matrix, in an amorphous state or the possibility of small crystals below the detection limit (Fouladian et al., 2020, Li et al., 2021).

3.2.3. SEM

The SEM images of pure 5FU, Cis, blank, and drug-loaded bilayer films are shown in Fig. 5. 5FU was found to exhibit a rough bulk-shaped appearance (Fig. 5A), whereas, Cis showed small geometric structures (Fig. 5B). Both blank films (Fig. 5C) and drug-loaded films (Fig. 5D) showed similar topographies with a slightly rough appearance. The fact that the blank film surface displays similar roughness as the drug-loaded film indicates that the roughness may not have been caused by the drugs' aggregates or crystallites and the drugs are fully dispersed in the film. These results comply with reported findings where 5FU and Cis-loaded films were found to exhibit relatively regular surfaces (Lei et al., 2010, Sonvico et al., 2018).

3.3. Quantification of 5FU and Cis by HPLC

The HPLC procedure quantified 5FU and Cis in their pure forms, release media, and 3DP films, eluting 5FU and Cis at 7.27 ± 0.28 min and 5.59 ± 0.03 min, respectively (Figure S4). The limits of detection and limit of quantitation using the aforementioned HPLC method were reported to be 0.10 and 0.25 μg/ml for 5-FU and 2.00 and 4.00 μg/ml for Cis, respectively.

3.4. Determination of drug content

The adopted extraction method was found to be accurate where the

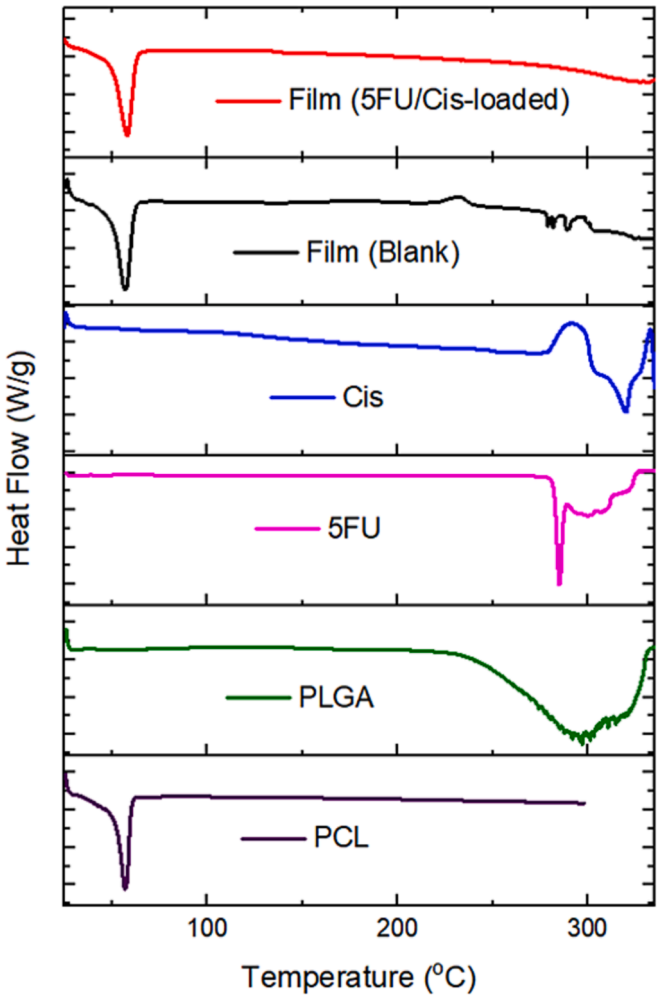

Fig. 4. Differential scanning calorimetry (DSC) thermograms of the 3DP bilayer films and their components.

extracted pure drugs showed R% of 98.69 ± 1.40 % and 102.86 ± 0.83 %, for 5FU and Cis, respectively. The drug content of films A, B, and C are summarized in Table 3. Since no established guidelines for determining loading doses of drug-eluting films, doses approaching potential maximum concentrations were selected, avoiding precipitation in the printing ink or after film drying. Subsequently, these doses were assessed for efficacy through experimental testing on HepG2 cell lines.

3.5. Determination of residual solvents

The incorporation of PCL and PLGA in the formulation required the use of solvents with strong solubilization powers, such as THF and DMF. Although these solvents were mostly removed by evaporation, residues might persist due to their incorporation within the polymer matrix and high boiling point of DMF (153 °C). Therefore, permissible levels of residual solvents are stated in United States Pharmacopeia (USP). Both solvents are considered class 2 solvents, indicating their concentrations should be limited in pharmaceutical products due to their inherent toxicities. USP recommends that the concentration limit of THF and DMF be 720 and 880 ppm, respectively (Convention, 2019). The tested films were selected to represent the highest printing infills for both layers thus indicating the maximum residual solvent amounts in the printed films. The results demonstrated that the concentration of THF was below 150 ppm, which corresponded to the lowest limit of quantitation of the applied GC method. On the other hand, residual DMF was quantified at 622.57 ± 4.59 ppm abiding by the USP guidelines confirming their safe use.

3.6. Determination of in vitro drug release profiles

3.6.1. Stability of 5FU and Cis in PBS

The analysis of 5FU and Cis in the release media is an integral step for establishing a drug's release profile, therefore their stability is essential to obtain accurate results. Table 4 summarizes the results of stability testing of 5FU and Cis where both drugs showed acceptable stability for 25 days in PBS at pH 7.4 and 6.9 (37 °C) with mean R% ranging from 96.48 to 99.99 % for 5FU and 99.82 – 103.07 % for Cis, all above 90% which abide by US FDA guidelines (Galanti et al., 2009).

3.6.2. In vitro release study

Films A, B, and C released their 5FU loads in 24 h, whereas Cis was released at a slower rate over 14–23 days (Fig. 6). The fast release of 5FU could be attributed to its high aqueous solubility (Fredenberg et al., 2011) (12.2 mg/ml for 5FU (Rider, 2007) versus 1.5 mg/ml for Cis (Kadokawa et al., 2021)). However, film B released its load at a slightly lower rate compared to films A and C which could be explained by the fact that layer 2 (Cis-loaded layer) backing 5FU loaded layer has a denser infill (40%), as opposed to 30% in the other films, which could have hindered the penetration of water within the polymer matrix causing the slower release of 5FU.

On the other hand, the release of Cis was found to be impacted significantly ($P < 0.005$) by the infill percentage. Cis load was released over 12, 14, and 23 days for films A, B, and C, respectively. Film B showed the slowest release rate (10%) compared to film A (13%) and film C (20%) after 24 h. Films A and C continued to exhibit similar release behavior, a total of 55% and 59% of Cis load were released during the following 5 days, respectively, compared to 40% from film B. Film C then completed releasing the remaining Cis load on day 12, whereas film A showed a slightly lower rate completing the release of the remaining load on day 14. Film B sustained the longest release duration of 23 days. An overall conclusion can be drawn that a higher infill % contributed to an extended and slower release when comparing films A and C (10% infill) to film B (15% infill). The findings agree with several reported results, demonstrating that products with denser designs release their drug load slower which is associated with a higher surface area, and volume ratio (McDonagh et al., 2022, Abdella et al., 2022). Although films A and C had the same infill percentage, film C showed a faster release. This could be due to the presence of the more porous 5FU backing layer facilitating the penetration of the release media to the Cis-loaded layer.

Studies have shown that cancerous tissues have a more acidic environment compared to healthy tissues, it was also found that the pH varies according to the cancer type (Abdella et al., 2023). Research conducted by Coman et al. on pH mapping of liver cancer reported pH values of 6.8, 6.9, and 7.2 for intratumoral, tumor edge, and liver parenchyma, respectively (Coman et al., 2020). An average pH of 6.9 was used to represent the microenvironment of liver cancer and the release profile of film A at pH 6.9 was compared to the pH 7.4 release profile, representing normal physiological conditions. The release profiles of both drugs did not show a substantial difference (Figure S5).

3.6.3. Mathematical modelling

The *in vitro* drug release behavior was compared to some mathematical models and the best-fitting model was considered where the highest R^2 and lower RMSE and AIC were obtained(Arafat et al., 2021). According to the results (Table S5), 5FU and Cis release from the studied films followed the Peppas-Sahlin model represented as (Amini-Fazl and Mobedi, 2020):

$$f = K_1 t^m + K_2 t^{2m}$$

m: Diffusional exponent

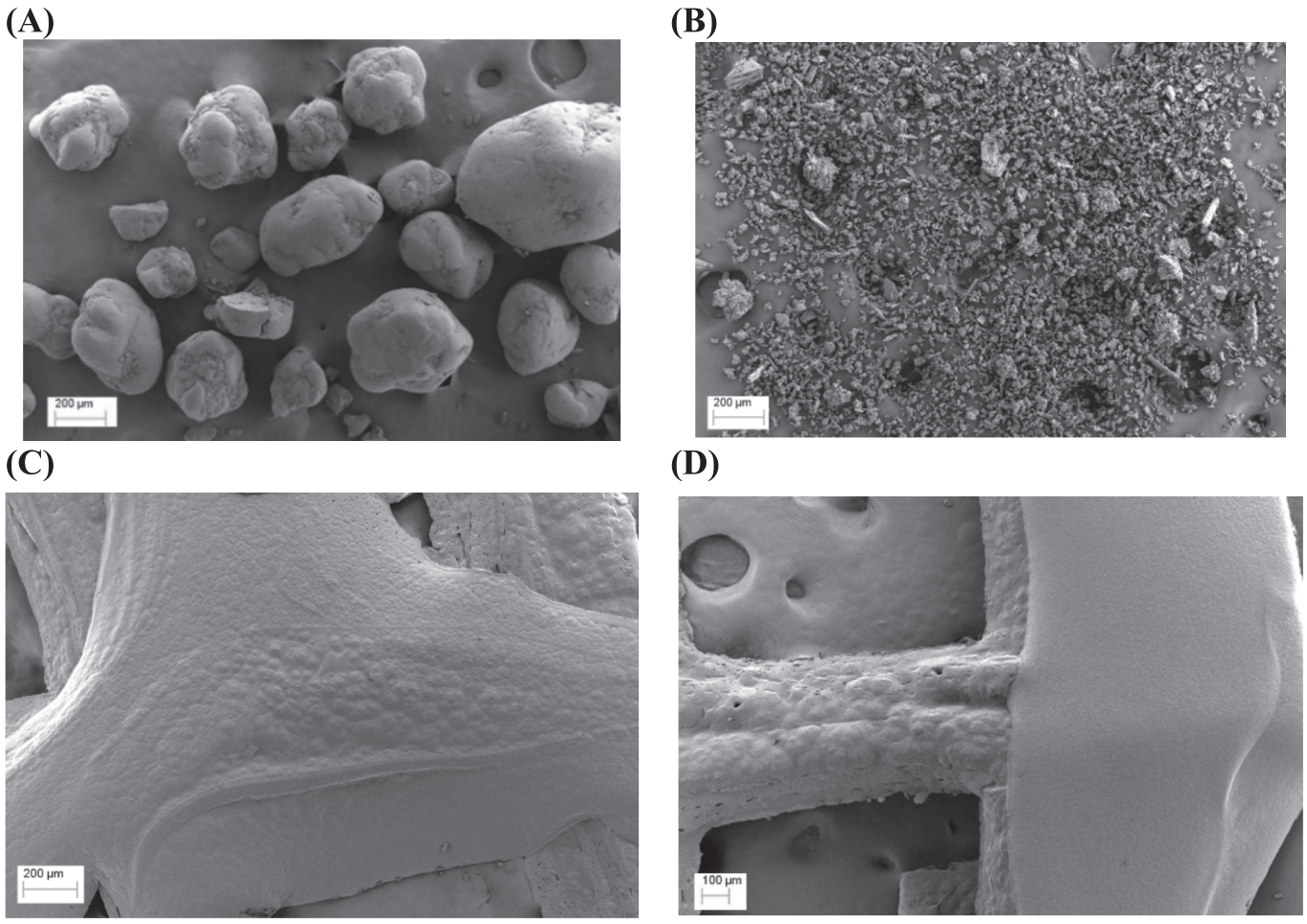

Fig. 5. Scanning Electron Microscopy images (x50 magnification) of (A) 5FU (B) Cis (C) Blank bilayer film and (D) Drug loaded bilayer film.

Table 3
The drugs content in each 3DP bilayer films (20 mm × 20 mm).

Formulation	Drug content (mg) per film (20 mm × 20 mm)	
	5FU	Cis
Film A	0.685 ± 0.017	0.392 ± 0.005
Film B	0.504 ± 0.002	0.800 ± 0.020
Film C	0.496 ± 0.001	0.339 ± 0.009

Table 4
The recovery percentages of 5FU and Cis in PBS at 37 °C at 7, 14, and 25 days.

	pH 7.4 (R % ± SD)		pH 6.9 (R % ± SD)	
Time (Days)	5FU	Cis	5FU	Cis
7	99.68 ± 2.68	101.89 ± 1.89	99.99 ± 1.97	100.95 ± 1.88
14	99.67 ± 0.39	103.07 ± 0.36	96.48 ± 1.26	99.82 ± 0.73
25	97.12 ± 0.18	99.93 ± 0.68	96.92 ± 1.63	101.33 ± 1.91

k_1: Fickian kinetics constant.

k_2: Non-Fickian kinetics constant.

This model indicates that drug release is governed by matrix relaxation and diffusion which complimented the nature of the developed films. The films consisted of biodegradable polymers, PCL, and PLGA, where release is regulated by water penetration which is achieved by the relaxation of the polymer matrix followed by drug diffusion (Lao et al., 2008). Peppas-Sahlin model considers the drug release during these stages thus providing a suitable prediction of the drug release profiles.

3.7. Stability studies

The stability of pharmaceutical products from the time of production to the time of administration is crucial to ensure patient safety, treatment efficacy, and overall integrity of the products. Since the proposed 3DP film is intended for personalized treatment, storage for extended periods was not necessary, the stability studies performed in this research determined the suitable storage conditions and suggested labeling instructions. The commonly used accelerated stability studies conditions at 40 °C were not used due to the low melting point of PCL (60 °C), where the films start to soften risking alterations in the dimensions of the pores of the films and possibly affecting the release profile of Cis. Therefore, ambient conditions were selected for storage of the films. The stability of the prepared films was determined based on changes in their drug content, FTIR, DSC, TGA, and mechanical profiles.

3.7.1. Drug content

The R% of 5FU and Cis in stored films relative to the initial drug content in freshly printed films are summarized in Table 5. Our results showed that both 5FU and Cis content in the printed films were above 90% of their initial concentration indicating their potency for at least 28 days at both storage conditions, as per US FDA guidelines (Galanti et al., 2009).

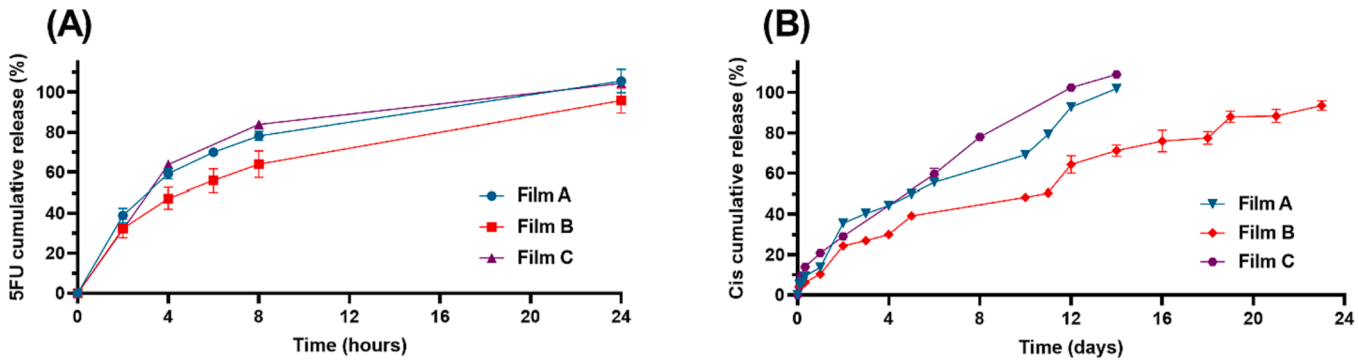

Fig. 6. In vitro cumulative release of 5FU and Cis from films A, B, and C (PBS, pH 7.4).

Table 5
Drugs content in 3DP films for 28 days under storage conditions (A) 25 °C and relative humidity of 60% (B) 4 °C.

	5FU (R% ± SD)		Cis (R% ± SD)	
Time (Days)	Storage conditions A	Storage conditions B	Storage conditions A	Storage conditions B
7	98.20 ± 0.33	95.00 ± 0.53	99.42 ± 0.60	97.96 ± 2.86
14	102.04 ± 0.90	98.24 ± 0.10	103.52 ± 0.38	102.66 ± 0.61
28	102.83 ± 0.25	98.48 ± 0.57	90.00 ± 0.38	± 0.51

3.7.2. FTIR

The FTIR charts of the stored films under both conditions were evaluated and compared with the freshly prepared films (Figure S6). All characteristic peaks which were determined previously under section 3.2.1. were detected for all films with no changes. Besides, no additional peaks were noted indicating the chemical stability of the films under the specified storage conditions and time intervals.

3.7.3. Thermal analysis

DSC charts for the stored films were evaluated in the second week at storage condition A and the fourth week at storage condition B (Fig. S7A). The DSC plots showed no endotherm peaks corresponding to 5FU or Cis peaks, indicating the stability of the films under the specified conditions and time intervals with no signs of drug crystallization. However, a small peak was observed at 310 °C for films stored at conditions B after 4 weeks. The peak could be attributed to the migration of TEC to the surface of the film upon storage (Budavari et al., 2004), DSC chart of pure TEC is shown in Fig. S7B.

Additionally, the thermal stability of the films was evaluated by TGA where the onset temperature (or the DTG maximum) obtained from the TGA (or DTG) curve implied the degradation or decomposition behavior thus their thermal stability (Loganathan et al., 2017). The TGA and DTG charts for the films are illustrated in Fig. S7C and S7D, respectively, the onset and DTG maximum temperatures were similar showing insignificant changes. Moreover, the glass transition temperature (T_g) indicates the physical stability of a product, T_g of the films was found to be 49.47 °C, 50.14 °C, and 50.96 °C for freshly printed films, films stored for two weeks under storage conditions A, and four weeks under storage conditions B, respectively. The T_g values showed insignificant changes suggesting that the tested storage conditions and durations had no impact on the physical stability of the printed films.

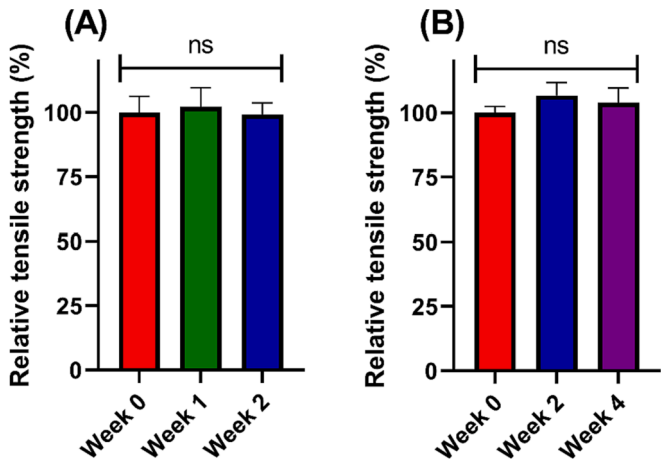

Fig. 7. Changes in the tensile strength of 3DP films stored in (A) Storage conditions A and (B) Storage conditions B.

3.7.4. Determination of tensile strength

Monitoring the change in the mechanical properties of the films during the storage period is necessary, to ensure the flexibility of the films at the time of use. Sufficient flexibility allows for maximum contact with the affected areas and enhances the efficiency of drug delivery The tensile strength of the printed films was determined for freshly printed films and compared to the films stored for 2 weeks (storage conditions A) and 4 weeks (storage conditions B). Fig. 7 showed that the changes in the tensile strength during the specified study period were not significant, and the films maintained their mechanical properties.

Considering the data obtained from the aforementioned stability studies, it can be concluded that the films demonstrated acceptable stability where drug content, physical characters, and mechanical properties were not altered significantly for 2 weeks upon storage at 25 °C / 60% relative humidity or 4 weeks upon refrigeration. Although the drug content was within acceptable limits at week 4, a significant decrease in tensile strength was observed in films stored under condition A after 4 weeks compared to freshly printed films. Consequently, the overall stability conclusion for condition A was established at 2 weeks.

3.8. Evaluation of cytotoxicity (MTS assay)

The cytotoxic effect of the films was evaluated by MTS assay using HepG2 cell lines, and the results were supported with microscopic imaging of the cells. Two approaches were adopted in MTS assays, extract dilution test (EDT) and direct contact test (DCT). The EDT involved exposing the HepG2 cells to the drug release extract of the tested films, whereas, in the DCT, the cells were exposed directly to the evaluated films, then cell viability was measured quantitively following both tests (Li et al., 2015). Although the EDT is commonly used, the DCT was reported to be more sensitive to detecting cytotoxicity and simulated physiological conditions more accurately (Baek et al., 2005). Fig. 8 shows a schematic diagram of the procedures used.

3.8.1. Extract dilution test

The cytotoxicity of 5FU and Cis released from 3DP bilayer films at different time points (2, 7, 14, and 23 days) against HepG2 cells were

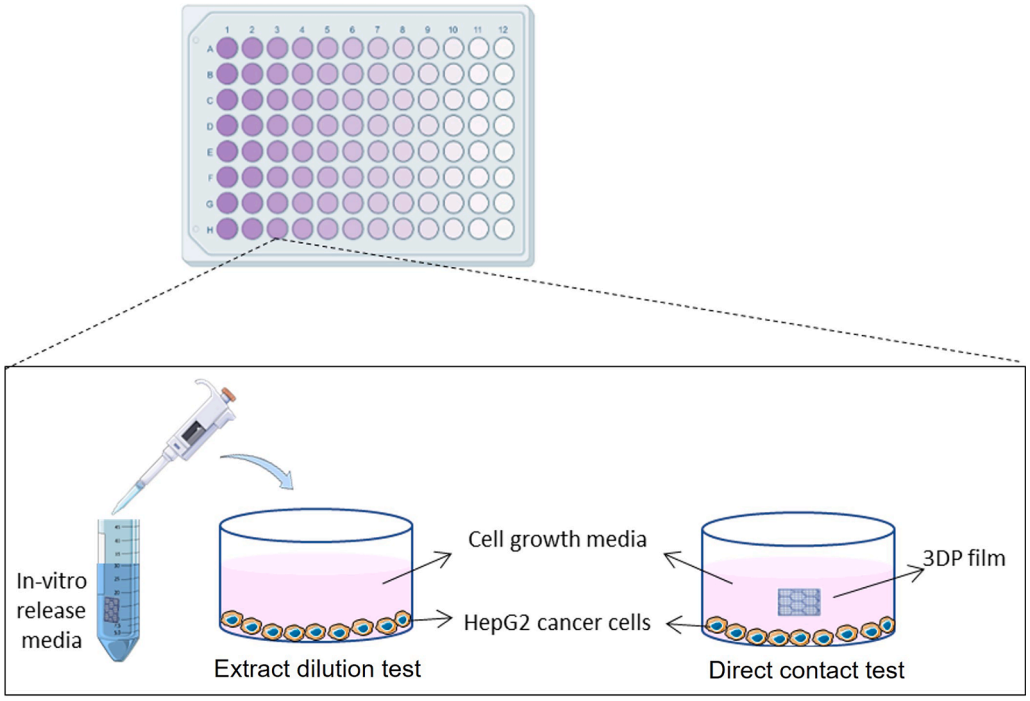

Fig. 8. Schematic diagram representing the experimental setup of extract dilution test and direct contact test (Parts of the figure were drawn using pictures from Servier Medical Art. Servier Medical Art by Servier is licensed under a Creative Commons Attribution 3.0 Unported License (https://creativecommons.org/licenses/by/3.0/ accessed on 3 July 2023).

measured. Two control groups were set up: untreated cells (control 1) and cells treated with blank film release media (control 2). Cell viability of control 2 did not show a substantial difference compared to control 1, excluding any possible cytotoxic effect by the components of the blank films. The MTS assay showed significant inhibition of HepG2 cell viability (Fig. 9A). The treated cells showed moderate cell death on day 2 (66% viability), which then significantly increased on day 23 (19% viability). The decrease in cell viability is time and concentration-dependent as the release medium from day 23 corresponding to higher cumulative drug concentration was more potent in killing HepG2 cells. Pure 5FU/Cis solutions with concentrations equivalent to that released at different time points were also tested on HepG2 cells and the apoptotic behavior did not show a significant difference to drugs released from the 3DP bilayer films indicating that the formulation process did not affect the cytotoxic ability of both drugs.

3.8.2. *Direct contact test*

Although EDT demonstrated the cytotoxic effect of the drug-loaded films, more accurate results could be obtained from DCT. In EDT, the amount of drug released dissolves in the surrounding release media,

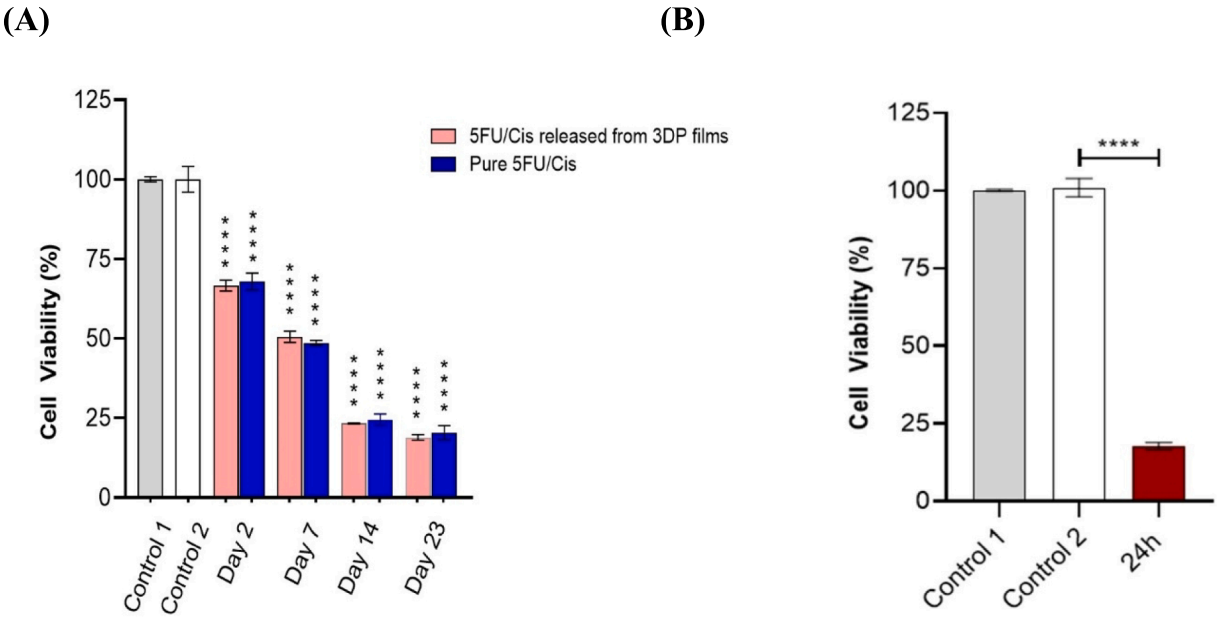

Fig. 9. Cytotoxic effects of 5FU/Cis (A) released from 3DP films (EDT) at different durations and the respective pure 5FU and Cis concentrations (positive control) on HepG2 cell line after 24 h treatment (B) directly released from 3DP bilayer films (DCT) on HepG2 cell line after 24 h treatment (**** $p < 0.0001$).

which is further diluted with cell culture media upon treatment. The concentration of 5FU and Cis in the diluted samples may not be sufficient to provide an accurate representation of their cytotoxicity. On the other hand, in DCT, the cells are directly exposed to the released drugs thereby offering a more realistic assessment of their potential cytotoxicity (Srivastava et al., 2017). The cell viability of untreated cells (Control 1) was similar to the blank film (Control 2), eliminating the possibility of the cells being crushed by the heaviness of the film and indicating no cytotoxicity was induced by the components of the blank films and the cell death would be attributed to the released drugs from the drug-loaded bilayer films (Fig. 9B). The results showed that cell viability was reduced significantly ($p < 0.0001$) upon direct treatment with the film after 24 h (19%).

3.8.3. Cell imaging

The morphology of the cells upon treatment in EDT and DCT was analyzed using the EVOS FL Cell Imaging System (Fig. 10A). The untreated HepG2 cells showed a characteristic epithelial-like morphology resembling control cells, indicating no effect of blank films on HepG2 cell viability. However, in the EDT, the cells treated with day 2 and day 7 release samples displayed reduced cell numbers with blebbing and shrunken cell morphology characteristic of apoptotic cells. The cells

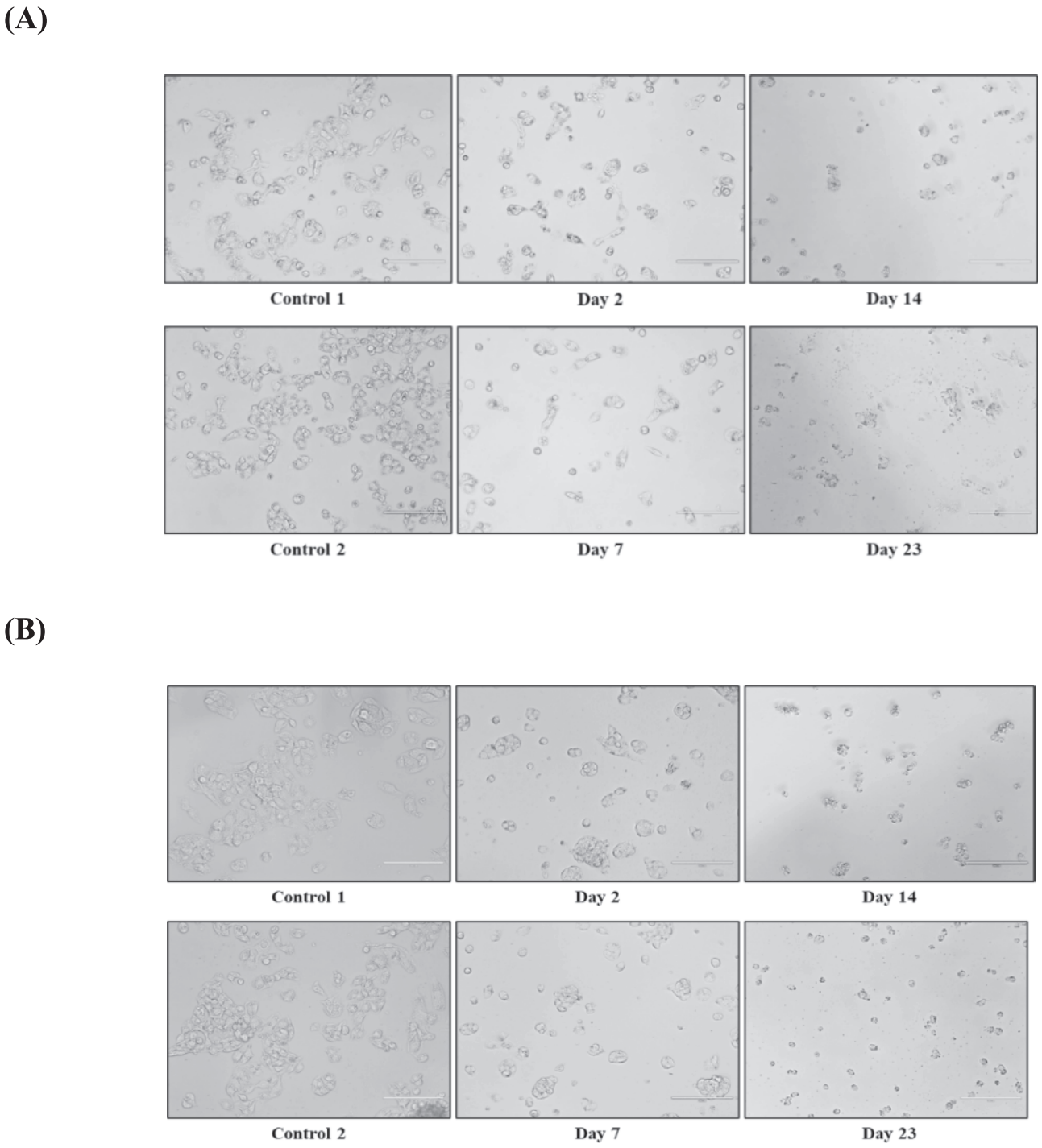

Fig. 10. Brightfield image of HepG2 cells at 20x upon treatment with (A) 5FU/Cis loaded-release samples from 3DP bilayer films at days 2, 7. 14, and 23 (B) Respective pure 5FU/Cis concentrations captured on EVOS FL at 24-hour post-treatment.

treated with day 14 and day 23 samples showed striking cytotoxicity and lost adhesion with increased apoptotic bodies, identical to HepG2 cell apoptosis demonstrated in previous reports (Liu et al., 2018). Interestingly, the morphological changes caused by the drug-loaded release medium (EDT) (Fig. 10A) resembled the changes inflicted by the pure drug mixture (Fig. 10B) signifying that cell death occurred in the same manner and the cytotoxic activity of the drugs was unaffected by the formulation process.

Similarly, the treated cells by DCT showed apoptotic phenotype at 24 h (Fig. 11), complementing the cell viability assay seen in Fig. 10, suggesting the effectiveness of the bilayer film in a setting simulating physiological conditions more accurately, where the cell culture solution acted as the release media and no dilution was performed.

In summary, both tests supported the finding that 3DP drug-loaded films showed increasing cytotoxic potential in HepG2 cells from the first day up to 23 days, which could be applied for the prevention of liver cancer recurrence.

3.9. IncuCyte cytotox green assay

Since the treatment of 5FU and Cis induced cell inhibition, the cell death upon exposure to these drugs in real-time by the IncuCyte live-cell imaging system using cytotox green was investigated. Cytotox Green is impermeable to healthy cells, however, upon induction of cell death and loss of membrane integrity, it can enter the cell and bind to the nuclei yielding a 100–1000-fold increase in green fluorescence (Fig. 12A-B). The dying cells are identified by the appearance of green-labeled nuclei over time and quantified using integrated analysis software (Fig. 12C-D).

HepG2 cells were treated with the drug-loaded release media collected on days 2, 7, 14, and 23 then the cell death was analyzed for up to 24 h. The control cell and the blank treatments showed similar cell proliferation as expected, supporting that the blank control does not interfere with cell growth and death, as previously observed in the MTS assay. The cytotox green accumulation was non-significant in the control and blank. However, the accumulation of cytotox green positive cells was noticeably increased from 0 to 24 h in days 2 and 7- treated cells compared to controls indicating that cell death was induced only upon the treatment. Moreover, the cytotox green positive cells were significantly higher on day 14 and reached the maximum on day 23 (Fig. 12A). The increase in cytotox green positive cells and the cell death accumulation was concentration-dependent, also complemented by the gradual increase of cytotox green intensity (Fig. 12C) supporting our MTS data from Fig. 9. Similarly, increased cell death was observed with direct exposure to the 3DP drug-loaded bilayer film, which was not seen in controls (Fig. 12B). The cytotox green intensity was significantly higher in treated cells by EDT (Fig. 12C) and DCT (Fig. 12D) compared to the controls.

3.10. Western blot

The apoptotic markers PARP and caspase 3 were tested by Western blotting. An increase in cleaved caspase −3 and PARP upon treating cells with both drugs-loaded release media and direct exposure to 3DP bilayer films was noted (Fig. 13A) which complements the cell death data from the MTS and Incucyte Cytotox Green assays as the cell death was directly proportional to the concentration of the drugs. Similar results were observed upon direct treatment of cells with 3DP bilayer films with no cleavage of caspase-3 or PARP by the controls (Fig. 13B).

3.11. Mitochondrial membrane potential

To determine whether 5FU and Cis treatment decreased cell survival by inducing apoptosis, we analyzed the reduction of mitochondrial inner membrane potential using tetramethyl-rhodamine ethyl ester (TMRE) staining. As shown in Fig. 14 a & b, HepG2 cells treated with 5FU/Cis had markedly reduced TMRE signal by both EDT and DCT methods, in a time-dependent manner, compared to untreated HepG2 cells. Our findings suggest that the 5FU/Cis 3DP bilayer films induced loss of mitochondrial membrane potential which promoted apoptosis in HepG2 cells.

3.12. Greenness assessment of the formulation development process

The development of the proposed 3DP bilayer film involved 2 main processes, analysis, and 3D printing which contribute to the generation of hazardous waste, consumption of energy, and other environmental concerns. Concurrent quantification of 5FU and Cis was performed by HPLC 1, The analysis of residual DMF by HPLC 2, and THF by GC. The HPLC 1 method was previously reported to score 82 points using the eco-scale tool (Youssef et al., 2021), however, the steps of sample preparation for determining the drug loading were not considered in that study. Therefore, the method was re-evaluated with the additional steps required for drug extraction, the steps involved the use of 1 ml DCM which resulted in the deduction of 2 penalty points (pp), giving the process an overall score of 80. On the other hand, the HPLC 2 method scored higher (86) than HPLC 1, where the mobile phase was composed of only one hazardous component (acetonitrile) and 95% sodium dihydrogen phosphate buffer which is a non-hazardous reagent versus SDS which encompasses three hazardous pictograms. Finally, the GC method scored the highest (93) of all three methods. Although higher energy consumption was evident, the use of a single reagent and low waste generation compensated for the elevated energy consumption. All the methods were considered “excellent green analysis” procedures as they scored above 75 points. While the eco-scale scores provided an easy way to evaluate the methods, they did not present the limitations of the method and did not consider all green analytical chemistry principles, thus the methods were further evaluated using AGREE tool. The scores generated by AGREE software showed the same score for HPLC 1 and 2 methods (0.62) with a corresponding green shade indicating good sustainable practices for the most part. On the other hand, GC scored 0.58 with a corresponding lighter green shade demonstrating more environmental concerns than HPLC methods. Although the scores for HPLC methods are equal, the pictogram highlighted that HPLC 2 was superior in terms of analysis throughput with more runs per hour due to its shorter run time compared to HPLC 1. Nonetheless, HPLC 1 required less

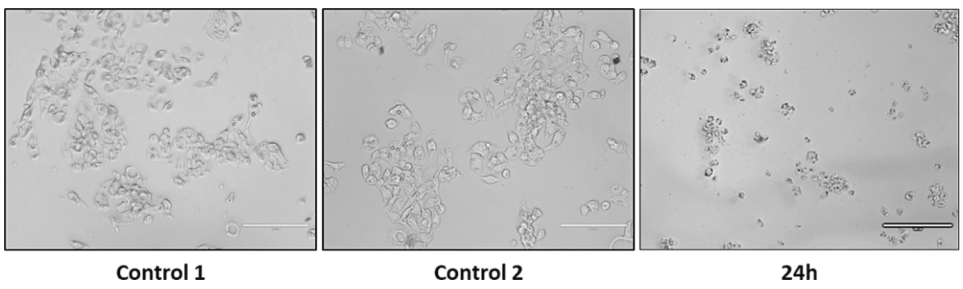

Fig. 11. Brightfield image of HepG2 cells at 20x upon treatment with 3DP bilayer films (DCT) captured on EVOS FL at 24 h post-treatment.

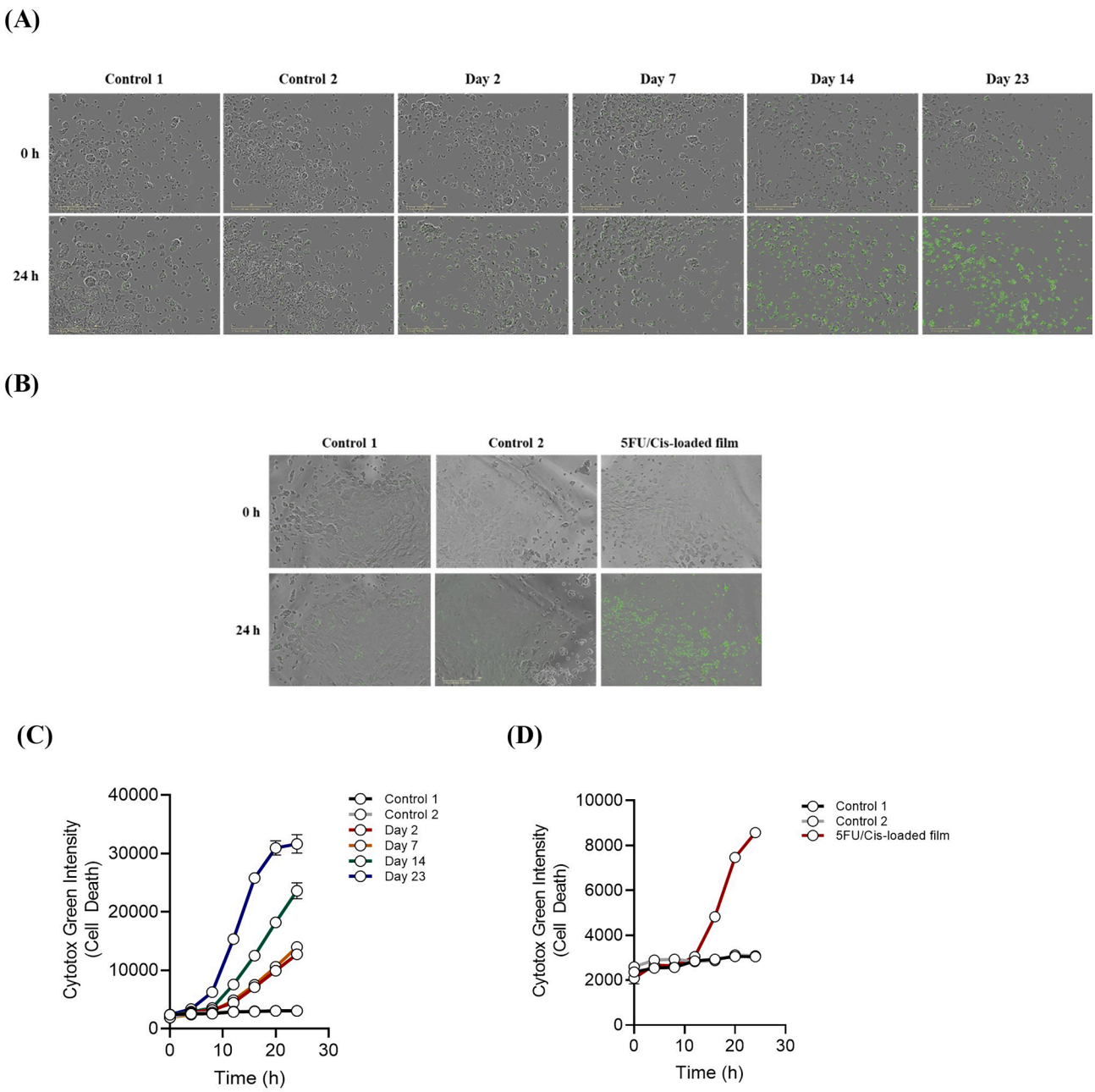

Fig. 12. The representative time-lapse images (0 h and 24 h) of HepG2 treated with (A) drug-loaded release media samples from 3DP bilayer films (EDT) (B) Direct 3DP bilayer films containing cytotox green. The cytotox green fluorescence intensity, which indicates cell death from (C) EDT and (D)DCT (calculated using Incucyte software, and the graphs were made in Prism GraphPad software). (For interpretation of the references to color in this figure legend, the reader is referred to the web version of this article.)

hazardous reagents namely, methanol and DCM versus sodium hydroxide and THF used in HPLC 2, scoring higher for operator's safety. Even though GC was superior considering the generation of less waste and the use of less hazardous reagents (acetone), the method was penalized for higher energy consumption and the absence of solvents from renewable sources, Table S6 summarizes the results.

Several factors dictate the final greenness assessment of the printing process, the iGAPP tool specific to the 3D printing of pharmaceutical products considers the different stages of printing (Youssef et al., 2022). Table S7 shows the breakdown of the greenness analysis of the used 3D printing process. Avoiding solvent removal during the pre-processing stage (sector 3), operating a bioprinter at a pressure lower than 110 kPa as opposed to other high-energy consuming printers (sector 5), generating no waste (sector 8), and adopting a non-energy consuming drying method (sector 9) contributed to high scoring and green shading in the iGAPP pictogram. Some intermediate green practices scored lower and were shaded yellow, such as the use of THF and DMF for the preparation of the printer feed (sector 1) which could not be avoided due to the hydrophobicity of the printed polymers. Also, points were deducted for the consumption of energy for dissolving the polymers (sector 2) and printing (sector 6), however, the minimum possible temperature was applied. The printing time of the films ranged from 7.5 min (film C) to 9 min (film A) where the maximum printing time was considered in the calculations. Finally, one red sector was demonstrated in the iGAPP pictogram (sector 10) which reflected on the long post-processing time of drying, nonetheless, a longer time was required to remove the residual solvents since drying was carried out at RT with no heated oven to maintain the integrity of the pore dimensions of the film.

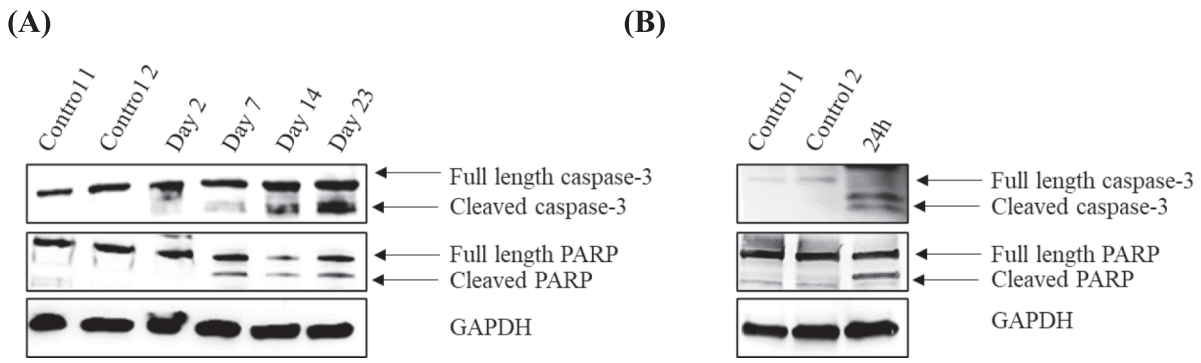

Fig. 13. The protein expression of cleaved caspase-3 and cleaved PAPR from HepG2 cells treated with (A) Drug-loaded release media at days 2,7,14, 23 and (B) Direct 3DP bilayer films by immunoblotting.

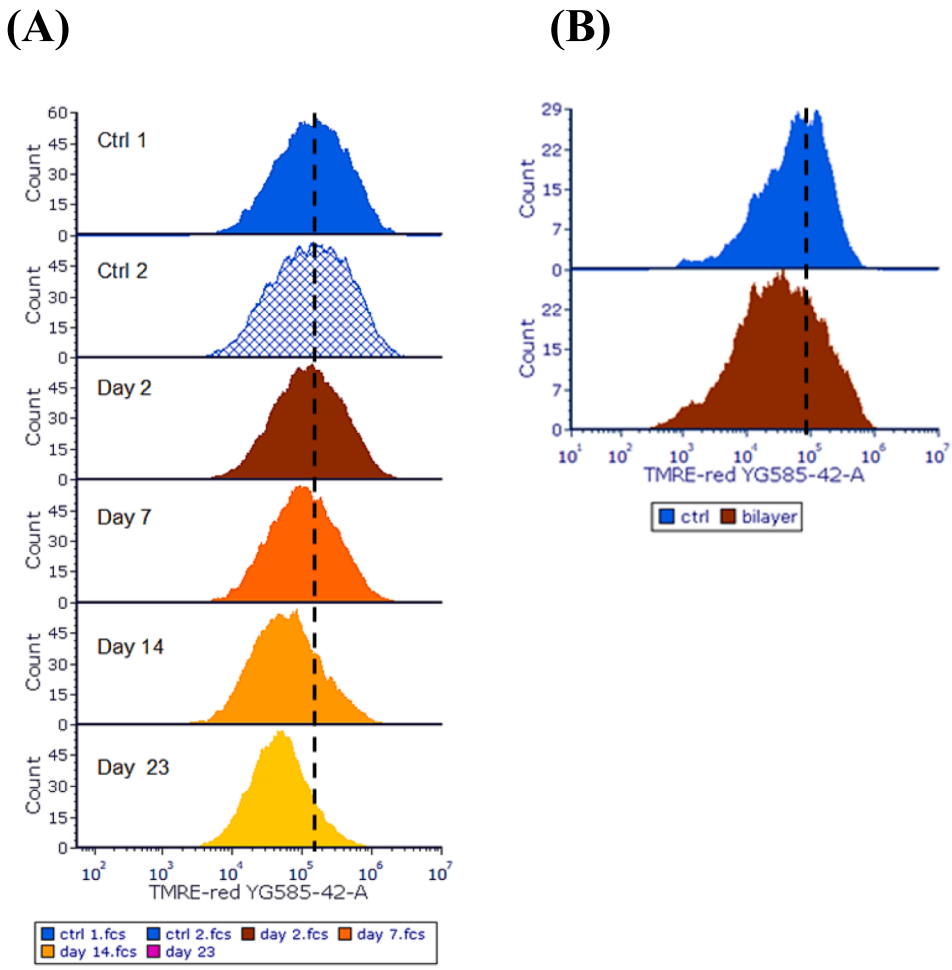

Fig. 14. The mitochondrial membrane potential of HepG2 cells treated with drug release medium by (A) Drug-loaded release media (EDT) at days 2,7,14, 23 and (B) Direct 3DP bilayer films (DCT) using 50 nM of TMRE and analyzed by Cytoflex S using the 561 nm laser-line and 585/42 bandpass filter. Histograms were normalized to the peak value of the control (untreated cells, solid blue). The dashed line illustrates the mean fluorescence intensity of the control (solid blue) data, for visual comparison. (For interpretation of the references to color in this figure legend, the reader is referred to the web version of this article.)

Overall, the printing procedure scored 7 which was considered a green process with a relatively low environmental impact.

4. Limitations and future direction

The developed 3DP film demonstrated potential in treatment of liver cancer, however, the 24-hour burst release of 5FU contrasted with the 23-day sustained release of Cis, might raise a concern regarding the optimal synergistic effect initiated by their concurrent administration. Given the limited availability of data on the pharmacokinetics of drugs administered through localized DDS such as films and implants, determining optimal doses and duration need more investigations. Therefore, further studies to determine the ideal release profiles of both drugs against hepatic carcinoma are necessary. Moreover, *in vivo* animal studies would contribute to establishing a correlation between tumor size and required dosing. Despite these concerns, the results from this

work could contribute to the development of an implant with optimized drug delivery efficiency for successful clinical application. Finally, the development of more greenness assessment tools to evaluate other procedures beyond analysis and 3D printing would be beneficial to allow the comparison of different protocols and application of modifications accordingly.

5. Conclusion

Adjuvant chemotherapy plays an important role in eradicating residual cancer cells after surgery thus reducing the risk of cancer recurrence. The uniqueness of every patient in terms of tumor size and shape, response to treatment, and required duration of treatment necessitates customized medications. This work described the development of a biodegradable 3DP bilayer film loaded with 5FU and Cis providing localized chemotherapy at the site of tumor resection. Different release profiles were achieved through altering the films' designs where 5FU was released over 24 h and Cis over 12–23 days. The films were evaluated for their cytotoxicity using HepG2 cells resulting in significant cell death (over 80%), showcasing the potential of the films in treating liver cancer. Complementing tests such as Wester Blots, TMRE staining, and live imaging confirmed cell death by apoptosis. Finally, the environmental impact of the analytical and printing methods was studied and modified accordingly to achieve minimal negative effects on the environment where possible and classified as excellent green practices using greenness assessment tools.

Funding statement.

CRediT authorship contribution statement

Souha H. Youssef: Conceptualization, Methodology & Investigation, Formal analysis, Validation, Visualization, Writing – original draft preparation. **Raja Ganesan:** Formal analysis, Methodology, Investigation, Writing – original draft preparation. **Marzieh Amirmostofian:** Methodology, Investigation, Writing – review & editing. **Sangseo Kim:** Formal analysis, Visualization, Writing – review & editing. **Ruhi Polara:** Investigation, Writing – review & editing. **Franklin Afinjuomo:** Writing – review & editing, Supervision. **Yunmei Song:** Conceptualization, Writing – review & editing, Supervision. **Bradley Chereda:** Formal analysis, Visualization. **Nimit Singhal:** Writing – review and editing, Supervision. **Nirmal Robinson:** Conceptualization, Writing – review and editing, Supervision. **Sanjay Garg:** Conceptualization, Writing – review and editing, Supervision.

Declaration of Competing Interest

The authors declare that they have no known competing financial interests or personal relationships that could have appeared to influence the work reported in this paper.

Data availability

Data will be made available on request.

Acknowledgement

The authors acknowledge the facilities, scientific and technical assistance of Microscopy Australia at the University of South Australia, a facility that is co-funded by the University of South Australia, the State and Federal Governments.

Funding statement

This research did not receive any specific grant from funding agencies in the public, commercial, or not-for-profit sectors.

Appendix A. Supplementary data

Supplementary data to this article can be found online at https://doi.org/10.1016/j.ijpharm.2024.123790.

References

Abdella, S., Youssef, S.H., Afinjuomo, F., Song, Y., Fouladian, P., Upton, R., Garg, S., 2021. 3D printing of thermo-sensitive drugs. Pharmaceutics. 13, 1524. https://doi.org/10.3390/pharmaceutics13091524.

Abdella, S., Afinjuomo, F., Song, Y., Upton, R., Garg, S., 2022. 3D printed bilayer mucoadhesive buccal film of estradiol: Impact of design on film properties, release kinetics and predicted in vivo performance. Int. J. Pharm. 628, 122324 https://doi.org/10.1016/j.ijpharm.2022.122324.

Abdella, S., Abid, F., Youssef, S.H., Kim, S., Afinjuomo, F., Malinga, C., Song, Y., Garg, S., 2023. pH and its applications in targeted drug delivery. Drug. Discov. Today. 28, 103414 https://doi.org/10.1016/j.drudis.2022.103414.

Alam, N., Khare, V., Dubey, R., Saneja, A., Kushwaha, M., Singh, G., Sharma, N., Chandan, B., Gupta, P.N., 2014. Biodegradable polymeric system for cisplatin delivery: Development, in vitro characterization and investigation of toxicity profile. Mater. Sci. Eng. C. 38, 85–93. https://doi.org/10.1016/j.msec.2014.01.043.

Alkahtani, S., Alarifi, S., Albasher, G., Al-Zharani, M., Aljarba, N.H., Almarzoug, M.H., Alhoshani, N.M., Al-Johani, N.S., Alothaid, H., Alkahtane, A.A., 2021. Poly Lactic-Co-Glycolic Acid- (PLGA-) Loaded Nanoformulation of Cisplatin as a Therapeutic Approach for Breast Cancers. Oxid. Med. Cell. Longev. 2021, 5834418. https://doi.org/10.1155/2021/5834418.

Amini-Fazl, M.S., Mobedi, H., 2020. Investigation of mathematical models based on diffusion control release for Paclitaxel from in-situ forming PLGA microspheres containing HSA microparticles. Mater. Technol. 35, 50–59. https://doi.org/10.1080/10667857.2019.1651549.

Ando, E., Tanaka, M., Yamashita, F., Kuromatsu, R., Yutani, S., Fukumori, K., Sumie, S., Yano, Y., Okuda, K., Sata, M., 2002. Hepatic arterial infusion chemotherapy for advanced hepatocellular carcinoma with portal vein tumor thrombosis. Cancer 95, 588–595. https://doi.org/10.1002/cncr.10694.

Andreadis, C., Vahtsevanos, K., Sidiras, T., Thomaidis, I., Antoniadis, K., Mouratidou, D., 2003. 5-Fluorouracil and cisplatin in the treatment of advanced oral cancer. Oral. Oncol. 39, 380–385. https://doi.org/10.1016/S1368-8375(02)00141-0.

Arafat, M., Fouladian, P., Wignall, A., Song, Y., Parikh, A., Albrecht, H., Prestidge, C.A., Garg, S., Blencowe, A., 2020. Development and in vitro evaluation of 5-fluorouracil-eluting stents for the treatment of colorectal cancer and cancer-related obstruction. Pharmaceutics. 13, 17. https://doi.org/10.3390/pharmaceutics13010017.

Arafat, M., Song, Y., Brewer, K., Fouladian, P., Parikh, A., Albrecht, H., Blencowe, A., Garg, S., 2021. Pharmaceutical Development of 5-Fluorouracil-Eluting Stents for the Potential Treatment of Gastrointestinal Cancers and Related Obstructions. Drug. Des. Devel. Ther. 15, 1495–1507. https://doi.org/10.2147/dddt.S299401.

Ashour, A.E., Badran, M., Kumar, A., Hussain, T., Alsarra, I.A., Yassin, A.E.B., 2019. Physical pegylation enhances the cytotoxicity of 5-fluorouracil-loaded PLGA and PCL nanoparticles. Int. J. Nanomed. 14, 9259. https://doi.org/10.2147/IJN.S223368.

Baek, H.S., Yoo, J.Y., Rah, D.K., Han, D.W., Lee, D.H., Kwon, O.H., Park, J.C., 2005. Evaluation of the extraction method for the cytotoxicity testing of latex gloves. Yonsei. Med. J. 46, 579–583.

Bassand, C., Benabed, L., Charlon, S., Verin, J., Freitag, J., Siepmann, F., Soulestin, J., Siepmann, J., 2023. 3D printed PLGA implants: APF DDM vs. FDM. J. Control. Release. 353, 864–874. https://doi.org/10.1016/j.jconrel.2022.11.052.

Belkhir, L., Elmeligi, A., 2019. Carbon footprint of the global pharmaceutical industry and relative impact of its major players. J. Clean. Prod. 214, 185–194. https://doi.org/10.1016/j.jclepro.2018.11.204.

Budavari, Z., Porkoláb, Z., Zelko, R., 2004. Study of triethyl citrate migration from coating polymers to tablet cores. Die Pharmazie-An International Journal of Pharmaceutical Sciences 59, 893–894.

Chan, K.L.A., Kazarian, S.G., 2006. Detection of trace materials with Fourier transform infrared spectroscopy using a multi-channel detector. Analyst 131, 126–131. https://doi.org/10.1039/B511243E.

Chen, W., Shi, K., Liu, J., Yang, P., Han, R., Pan, M., Yuan, L., Fang, C., Yu, Y., Qian, Z., 2023. Sustained co-delivery of 5-fluorouracil and cis-platinum via biodegradable thermo-sensitive hydrogel for intraoperative synergistic combination chemotherapy of gastric cancer. Bioact. Mater. 23, 1–15. https://doi.org/10.1016/j.bioactmat.2022.10.004.

Chidambaram, M., Manavalan, R., Kathiresan, K., 2011. Nanotherapeutics to overcome conventional cancer chemotherapy limitations. J. Pharm. Pharm. Sci. 14, 67–77.

Coman, D., Peters, D.C., Walsh, J.J., Savic, L.J., Huber, S., Sinusas, A.J., Lin, M., Chapiro, J., Constable, R.T., Rothman, D.L., Duncan, J.S., Hyder, F., 2020. Extracellular pH mapping of liver cancer on a clinical 3T MRI scanner. Magn. Reson. Med. 83, 1553–1564. https://doi.org/10.1002/mrm.28035.

Di Luca, M., Hoskins, C., Corduas, F., Onchuru, R., Oluwasanmi, A., Mariotti, D., Conti, B., Lamprou, D.A., 2022. 3D printed biodegradable multifunctional implants for effective breast cancer treatment. Int. J. Pharm. 629, 122363 https://doi.org/10.1016/j.ijpharm.2022.122363.

Ding, A.G., Schwendeman, S.P., 2008. Acidic microclimate pH distribution in PLGA microspheres monitored by confocal laser scanning microscopy. Pharm. Res. 25, 2041–2052. https://doi.org/10.1007/s11095-008-9594-3.

Ebrahimi Shahmabadi, H., Movahedi, F., Koohi Moftakhari Esfahani, M., Alavi, S.E., Eslamifar, A., 2014. Efficacy of Cisplatin-loaded polybutyl cyanoacrylate

nanoparticles on the glioblastoma. Tumour. Biol. 35, 4799–4806. https://doi.org/10.1007/s13277-014-1630-9.
Elbadawi, M., Basit, A.W., Gaisford, S., 2023. Energy consumption and carbon footprint of 3D printing in pharmaceutical manufacture. Int. J. Pharm. 639, 122926 https://doi.org/10.1016/j.ijpharm.2023.122926.
Fouladian, P., Kohlhagen, J., Arafat, M., Afinjuomo, F., Workman, N., Abuhelwa, A.Y., Song, Y., Garg, S., Blencowe, A., 2020. Three-dimensional printed 5-fluorouracil eluting polyurethane stents for the treatment of oesophageal cancers. Biomater. Sci. 8, 6625–6636. https://doi.org/10.1039/D0BM01355B.
Fredenberg, S., Wahlgren, M., Reslow, M., Axelsson, A., 2011. The mechanisms of drug release in poly(lactic-co-glycolic acid)-based drug delivery systems—A review. Int. J. Pharm. 415, 34–52. https://doi.org/10.1016/j.ijpharm.2011.05.049.
Galanti, L., Lebitasy, M.P., Hecq, J.D., Cadrobbi, J., Vanbeckbergen, D., Jamart, J., 2009. Long-term stability of 5-Fluorouracil in 0.9% sodium chloride after freezing, microwave thawing, and refrigeration. Can. J. Hosp. Pharm. 62, 34–38. https://doi.org/10.4212/cjhp.v62i1.115.
Gałuszka, A., Migaszewski, Z.M., Konieczka, P., Namieśnik, J., 2012. Analytical Eco-Scale for assessing the greenness of analytical procedures. TrAC. 37, 61–72. https://doi.org/10.1016/j.trac.2012.03.013.
Gentile, P., Chiono, V., Carmagnola, I., Hatton, P.V., 2014. An overview of poly(lactic-co-glycolic) acid (PLGA)-based biomaterials for bone tissue engineering. Int. J. Mol. Sci. 15, 3640–3659.
Heimbach, J.K., Kulik, L.M., Finn, R.S., Sirlin, C.B., Abecassis, M.M., Roberts, L.R., Zhu, A.X., Murad, M.H., Marrero, J.A., 2018. AASLD guidelines for the treatment of hepatocellular carcinoma. Hepatology 67, 358–380. https://doi.org/10.1002/hep.29086.
Inchingolo, R., Posa, A., Mariappan, M., Spiliopoulos, S., 2019. Locoregional treatments for hepatocellular carcinoma: Current evidence and future directions. World. J. Gastroenterol. 25, 4614–4628.
Isaacson, C., Mohr, T.K.G., Field, J.A., 2006. Quantitative Determination of 1,4-Dioxane and Tetrahydrofuran in Groundwater by Solid Phase Extraction GC/MS/MS. Environ. Sci. Tech. 40, 7305–7311.
Jing, Z., Ni, R., Wang, J., Lin, X., Fan, D., Wei, Q., Zhang, T., Zheng, Y., Cai, H., Liu, Z., 2021. Practical strategy to construct anti-osteosarcoma bone substitutes by loading cisplatin into 3D-printed titanium alloy implants using a thermosensitive hydrogel. Bioact. Mater. 6, 4542–4557. https://doi.org/10.1016/j.bioactmat.2021.05.007.
Kadokawa, R., Fujie, T., Sharma, G., Ishibashi, K., Ninomiya, K., Takahashi, K., Hirata, E., Kuroda, K., 2021. High loading of trimethylglycine promotes aqueous solubility of poorly water-soluble cisplatin. Sci. Rep. 11, 9770. https://doi.org/10.1038/s41598-021-89144-0.
Kanetaka, K., Enjoji, A., Furui, J., Nagata, Y., Fujioka, H., Shiogama, T., Miyata, A., Kishikawa, H., Matsuo, S., Iwata, T., Kanematsu, T., Eguchi, S., 2012. Effects of intermittent 5-fluorouracil and low-dose cisplatin therapy on advanced and recurrent gastric cancer. Anticancer. Res. 32, 3495–3499.
Karbownik, A., Szałek, E., Urjasz, H., Głęboka, A., Mierzwa, E., Grześkowiak, E., 2012. The physical and chemical stability of cisplatin (Teva) in concentrate and diluted in sodium chloride 0.9%. Contemp. Oncol. 16, 435–439.
Karki, S., Kim, H., Na, S.-J., Shin, D., Jo, K., Lee, J., 2016. Thin films as an emerging platform for drug delivery. Asian. J. Pharm. Sci. 11, 559–574. https://doi.org/10.1016/j.ajps.2016.05.004.
Kawai, T., Goumard, C., Jeune, F., Savier, E., Vaillant, J.C., Scatton, O., 2018. Laparoscopic liver resection for colorectal liver metastasis patients allows patients to start adjuvant chemotherapy without delay: a propensity score analysis. Surg. Endosc. 32, 3273–3281. https://doi.org/10.1007/s00464-018-6046-y.
Kengo, K., Akihito, E., Junichiro, F., Yasuhiro, N., Hikaru, F., Toshiaki, S., Akimi, M., Hiroki, K., Shigetoshi, M., Toru, I., Takashi, K., Susumu, E. & The Nagasaki Study Group for Digestive Organ Cancer, C., 2012. Effects of intermittent 5-fluorouracil and low-dose cisplatin therapy on advanced and recurrent gastric cancer. Anticancer Res.. 32, 3495.
Kobayashi, K., Tsuji, A., Morita, S., Horimi, T., Shirasaka, T., Kanematsu, T., 2006. A phase II study of LFP therapy (5-FU (5-fluorourasil) continuous infusion (CVI) and Low-dose consecutive (Cisplatin) CDDP) in advanced biliary tract carcinoma. phase II study of LFP therapy (5-FU (5-fluorourasil) continuous infusion (CVI) and Low-dose consecutive (Cisplatin) CDDP) in advanced biliary tract carcinomaEuropean. J. Pharm. Biopharma. 6, 121. https://doi.org/10.1186/1471-2407-6-121.
Kudo, M., Ueshima, K., Yokosuka, O., Ogasawara, S., Obi, S., Izumi, N., Aikata, H., Nagano, H., Hatano, E., Sasaki, Y., Hino, K., Kumada, T., Yamamoto, K., Imai, Y., Iwadou, S., Ogawa, C., Okusaka, T., Kanai, F., Akazawa, K., Yoshimura, K.-I., Johnson, P., Arai, Y., Kudo, M., Ueshima, K., Yokosuka, O., Ogasawara, S., Obi, S., Izumi, N., Aikata, H., Nagano, H., Hatano, E., Sasaki, Y., Hino, K., Kumada, T., Yamamoto, K., Imai, Y., Iwadou, S., Ogawa, C., Okusaka, T., Kanai, F., Akazawa, K., Yoshimura, K.-I., Johnson, P., Arai, Y., 2018. Sorafenib plus low-dose cisplatin and fluorouracil hepatic arterial infusion chemotherapy versus sorafenib alone in patients with advanced hepatocellular carcinoma (SILIUS): a randomised, open label, phase 3 trial. Lancet. Gastroenterol. Hepatol. 3, 424–432. https://doi.org/10.1016/S2468-1253(18)30078-5.
Lao, L.L., Venkatraman, S.S., Peppas, N.A., 2008. Modeling of drug release from biodegradable polymer blends. Eur. J. Pharm. Biopharm. 70, 796–803. https://doi.org/10.1016/j.ejpb.2008.05.024.
Lazaros, L., Dimitrios, T., Nikolaos, P., Christos, P., George, K., Stamatina, D., Anna, E., 2012. Salvage Chemotherapy with Cisplatin and 5-Fluorouracil in Metastatic Breast Cancer. Particular Activity against Liver Metastases. Anticancer. Res 32, 1833.
Lei, L., Liu, X., Guo, S., Tang, M., Cheng, L., Tian, L., 2010. 5-Fluorouracil-loaded multilayered films for drug controlled releasing stent application: Drug release, microstructure, and ex vivo permeation behaviors. J. Control. Release. 146, 45–53. https://doi.org/10.1016/j.jconrel.2010.05.017.
Li, R., Song, Y., Fouladian, P., Arafat, M., Chung, R., Kohlhagen, J., Garg, S., 2021. Three-Dimensional Printing of Curcumin-Loaded Biodegradable and Flexible Scaffold for Intracranial Therapy of Glioblastoma Multiforme. Pharmaceutics. 13, 471.
Li, W., Zhou, J., Xu, Y., 2015. Study of the in vitro cytotoxicity testing of medical devices. Biomed. Rep. 3, 617–620. https://doi.org/10.3892/br.2015.481.
Lim, S.H., Kathuria, H., Tan, J.J.Y., Kang, L., 2018. 3D printed drug delivery and testing systems — a passing fad or the future? Adv. Drug. Deliv. Rev. 132, 139–168. https://doi.org/10.1016/j.addr.2018.05.006.
Liu, Z., Sun, X., Xiao, S., Lin, Y., Li, C., Hao, N., Zhou, M., Deng, R., Ke, S., Zhong, Z., 2018. Characterization of aptamer-mediated gene delivery system for liver cancer therapy. Oncotarget 9, 6830–6840. https://doi.org/10.18632/oncotarget.23564.
Loganathan, S., Valapa, R. B., Mishra, R. K., Pugazhenthi, G. & Thomas, S. 2017. Chapter 4 - Thermogravimetric Analysis for Characterization of Nanomaterials. In: Thomas, S., Thomas, R., Zachariah, A. K. & Mishra, R. K. (Eds.) Thermal and Rheological Measurement Techniques for Nanomaterials Characterization. Elsevier.
Lubel, J.S., Roberts, S.K., Strasser, S.I., Thompson, A.J., Philip, J., Goodwin, M., Clarke, S., Crawford, D.H., Levy, M.T., Shackel, N., 2021. Australian recommendations for the management of hepatocellular carcinoma: a consensus statement. Med. J. Aust. 214, 475–483.
Marrero, J.A., Kulik, L.M., Sirlin, C.B., Zhu, A.X., Finn, R.S., Abecassis, M.M., Roberts, L. R., Heimbach, J.K., 2018. Diagnosis, Staging, and Management of Hepatocellular Carcinoma: 2018 Practice Guidance by the American Association for the Study of Liver Diseases. Hepatology 68, 723–750.
McDonagh, T., Belton, P., Qi, S., 2022. An investigation into the effects of geometric scaling and pore structure on drug dose and release of 3D printed solid dosage forms. Eur. J. Pharm. Biopharm. 177, 113–125. https://doi.org/10.1016/j.ejpb.2022.06.013.
Nishioka, Y., Moriyama, J., Matoba, S., Kuroyanagi, H., Hashimoto, M., Shindoh, J., 2018. Prognostic Impact of Adjuvant Chemotherapy after Hepatic Resection for Synchronous and Early Metachronous Colorectal Liver Metastases. Dig. Surg. 35, 187–195.
Nordlinger, B., Sorbye, H., Glimelius, B., Poston, G.J., Schlag, P.M., Rougier, P., Bechstein, W.O., Primrose, J.N., Walpole, E.T., Finch-Jones, M., Jaeck, D., Mirza, D., Parks, R.W., Mauer, M., Tanis, E., Van Cutsem, E., Scheithauer, W., Gruenberger, T., 2013. Perioperative FOLFOX4 chemotherapy and surgery versus surgery alone for resectable liver metastases from colorectal cancer (EORTC 40983): long-term results of a randomised, controlled, phase 3 trial. Lancet. Oncol. 14, 1208–1215. https://doi.org/10.1016/S1470-2045(13)70447-9.
Okamura, M., Hashimoto, K., Shimada, J., Sakagami, H., 2004. Apoptosis-inducing activity of cisplatin (CDDP) against human hepatoma and oral squamous cell carcinoma cell lines. Anticancer. Res. 24, 655–661. https://pubmed.ncbi.nlm.nih.gov/15161008/.
Pan, M., Huang, T., Xu, Z., Luo, W., Yang, Y., Teng, T., Huang, H., 2023. Absorbable 3D-printed pancreaticojejunostomy device with a dual-layer drug coating for the prevention of postoperative local recurrence of pancreatic cancer. J. Mater. Sci. Technol. 154, 178–188. https://doi.org/10.1016/j.jmst.2023.01.016.
Pena-Pereira, F., Wojnowski, W., Tobiszewski, M., 2020. AGREE—Analytical GREEnness metric approach and software. Anal. Chem. 92, 10076–10082. https://doi.org/10.1021/acs.analchem.0c01887.
Pinna, A.D., Yang, T., Mazzaferro, V., De Carlis, L., Zhou, J., Roayaie, S., Shen, F., Sposito, C., Cescon, M., Di Sandro, S., 2018. Liver transplantation and hepatic resection can achieve cure for hepatocellular carcinoma. Ann. Surg. 268, 868–875. https://doi.org/10.1097/SLA.0000000000002889.
Preis, M., Breitkreutz, J., Sandler, N., 2015. Perspective: Concepts of printing technologies for oral film formulations. Int. J. Pharm. 494, 578–584. https://doi.org/10.1016/j.ijpharm.2015.02.032.
Qiao, X., Yang, Y., Huang, R., Shi, X., Chen, H., Wang, J., Chen, Y., Tan, Y., Tan, Z., 2019. E-Jet 3D-Printed Scaffolds as Sustained Multi-Drug Delivery Vehicles in Breast Cancer Therapy. J. Pharm. Res. 36, 182. https://doi.org/10.1007/s11095-019-2687-3.
Repka, M.A., Gutta, K., Prodduturi, S., Munjal, M., Stodghill, S.P., 2005. Characterization of cellulosic hot-melt extruded films containing lidocaine. Eur. J. Pharm. Biopharm. 59, 189–196. https://doi.org/10.1016/j.ejpb.2004.06.008.
Rider, B.J. 2007. 5 Fluorouracil. In: Enna, S J., Bylund, D. B. (eds.) xPharm: The Comprehensive Pharmacology Reference. New York: Elsevier.
Salmoria, G., Vieira, F., Ghizoni, G., Marques, M., Kanis, L., 2017. 3D printing of PCL/Fluorouracil tablets by selective laser sintering: Properties of implantable drug delivery for cartilage cancer treatment. Rheumatol. Orthop. Med. 4.
Schwendeman, S.P., 2002. Recent advances in the stabilization of proteins encapsulated in injectable PLGA delivery systems. Crit. Rev. Ther. Drug. Carrier. Syst. 19 https://doi.org.10.1615/critrevtherdrugcarriersyst.v19.i1.20.
Sherman, M., Burak, K., Maroun, J., Metrakos, P., Knox, J.J., Myers, R.P., Guindi, M., Porter, G., Kachura, J.R., Rasuli, P., Gill, S., Ghali, P., Chaudhury, P., Siddiqui, J., Valenti, D., Weiss, A., Wong, R., 2011. Multidisciplinary Canadian consensus recommendations for the management and treatment of hepatocellular carcinoma. Curr. Oncol. 18, 228–240.
Siegel, R.L., Miller, K.D., Jemal, A., 2019. Cancer statistics, 2019. CA. Cancer. J. Clin. 69, 7–34. https://doi.org/10.3322/caac.21551.
Sonvico, F., Barbieri, S., Colombo, P., Mucchino, C., Barocelli, E., Cantoni, A.M., Cavazzoni, A., Petronini, P.G., Rusca, M., Carbognani, P., Ampollini, L., 2018. Physicochemical and pharmacokinetic properties of polymeric films loaded with cisplatin for the treatment of malignant pleural mesothelioma. J. Thorac. Dis. 10, S194–S206. https://doi.org/10.21037/jtd.2017.10.12.
Srivastava, G., García-Gutiérrez, M. & Pastor, J., 2017. Direct contact method with new technical steps essential to detect cytotoxicity of a volatile substance. Medical device

quality assurance. J. Allbiosolution. https://www.allbiosolution.com/2017/12/direct-contact-method-with-crucial.html.

Terashima, M., Irinoda, T., Kawamura, H., Takagane, A., Abe, K., Oyama, K., Fujiwara, H., Saito, K., Gotoh, M., Shirasaka, T., 2003. Intermittent FLDP: 24-h infusion of 5-FU on days 1, 3 and 5 combined with low-dose cisplatin on days 1–5 for gastric cancer, and its pharmacologic and kinetic rationale. Cancer. Chemother. Pharmacol. 51, 240–246. https://doi.org/10.1007/s00280-003-0568-1.

Tsilimigras, D.I., Hyer, J.M., Paredes, A.Z., Moris, D., Sahara, K., Guglielmi, A., Aldrighetti, L., Weiss, M., Bauer, T.W., Alexandrescu, S., Poultsides, G.A., Maithel, S. K., Marques, H.P., Martel, G., Pulitano, C., Shen, F., Soubrane, O., Koerkamp, B.G., Endo, I., Sasaki, K., Aucejo, F., Zhang, X.F., Pawlik, T.M., 2021. Tumor Burden Dictates Prognosis Among Patients Undergoing Resection of Intrahepatic Cholangiocarcinoma: A Tool to Guide Post-Resection Adjuvant Chemotherapy? Ann. Surg. Oncol. 28, 1970–1978. https://doi.org/10.1245/s10434-020-09393-7.

Ueshima, K., Kudo, M., Takita, M., Nagai, T., Tatsumi, C., Ueda, T., Kitai, S., Ishikawa, E., Yada, N., Inoue, T., Hagiwara, S., Minami, Y., Chung, H., 2010. Hepatic Arterial Infusion Chemotherapy Using Low-Dose 5-Fluorouracil and Cisplatin for Advanced Hepatocellular Carcinoma. Oncology 78, 148–153. https://doi.org/10.1159/000315244.

United States Pharmacopeial Convention, 2019. Residual Solvents. https://www.uspnf.com/sites/default/files/usp_pdf/EN/USPNF/revisions/gc-467-residual-solvents-ira-20190927.pdf. (16/10/2022).

Wang, Y., Wang, Z.Q., Wang, F.H., Yuan, Y.F., Li, B.K., Ding, P.R., Chen, G., Wu, X.J., Lu, Z.H., Pan, Z.Z., Wan, D.S., Sun, P., Yan, S.M., Xu, R.H., Li, Y.H., 2017. The role of adjuvant chemotherapy for colorectal liver metastasectomy after pre-operative chemotherapy: is the treatment worthwhile? J. Cancer. 8, 1179–1186. https://doi.org/10.7150/jca.18091.

Wang, Y., Sun, L., Mei, Z., Zhang, F., He, M., Fletcher, C., Wang, F., Yang, J., Bi, D., Jiang, Y., 2020. 3D printed biodegradable implants as an individualized drug delivery system for local chemotherapy of osteosarcoma. Mater. Des. 186, 108336 https://doi.org/10.1016/j.matdes.2019.108336.

Yang, Y., Qiao, X., Huang, R., Chen, H., Shi, X., Wang, J., Tan, W., Tan, Z., 2020. E-jet 3D printed drug delivery implants to inhibit growth and metastasis of orthotopic breast cancer. Biomaterials 230, 119618. https://doi.org/10.1016/j.biomaterials.2019.119618.

Yi, H.-G., Choi, Y.-J., Kang, K.S., Hong, J.M., Pati, R.G., Park, M.N., Shim, I.K., Lee, C.M., Kim, S.C., Cho, D.-W., 2016. A 3D-printed local drug delivery patch for pancreatic cancer growth suppression. J. Control. Release. 238, 231–241. https://doi.org/10.1016/j.jconrel.2016.06.015.

Youssef, S.H., Afinjuomo, F., Song, Y., Garg, S., 2021. Development of a novel chromatographic method for concurrent determination of 5-fluorouracil and cisplatin: Validation, greenness evaluation, and application on drug-eluting film. Microchem. J. 168, 106510 https://doi.org/10.1016/j.microc.2021.106510.

Youssef, S.H., Abdella, S., Garg, S., 2022. Development and Validation of a Novel Tool for Assessing the Environmental Impact of 3D Printing Technologies: A Pharmaceutical Perspective. Pharmaceutics. 14, 933.

Youssef, S.H., Kim, S., Khetan, R., Afinjuomo, F., Song, Y., Garg, S., 2023. The development of 5-fluorouracil biodegradable implants: A comparative study of PCL/PLGA blends. J. Drug. Delivery. Sci. Technol. 81, 104300 https://doi.org/10.1016/j.jddst.2023.104300.

Zhang, Y., Liu, S., Wang, X., Zhang, Z.-Y., Jing, X.-B., Zhang, P., Xie, Z.-G., 2014. Prevention of local liver cancer recurrence after surgery using multilayered cisplatin-loaded polylactide electrospun nanofibers. Chin. J. Polym. Sci. 32, 1111–1118. https://link.springer.com/article/10.1007/s10118-014-1491-0.